Immunity & Ageing

RESEARCH

Open Access

Elocalcitol mitigates high-fat diet-induced microglial senescence via miR-146a modulation

Keerthana Chithanathan[1], Monika Jürgenson[1], Katrina Ducena[2], Anu Remm[3], Kalev Kask[4], Ana Rebane[3], Li Tian[5] and Alexander Zharkovsky[1*]

Abstract

Background MicroRNAs (miRNAs) play crucial roles in regulating inflammation and cellular senescence. Among them, miR-146a has emerged as a key modulator of inflammation, but its role in obesity-induced senescence remains unexplored. This study investigates the involvement of miR-146a in high-fat diet (HFD)-induced hypothalamic senescence and in protective effects of elocalcitol (Elo), a non-hypercalcemic, fluorinated vitamin D analog on HFD-induced senescence.

Results Wild-type (*WT*) HFD-fed mice exhibited increased body weight, impaired locomotor activity, and cognitive decline compared to low-fat diet (LFD) controls. In the brain, HFD induced senescence markers (*p16*, *p21*), β-galactosidase activity (β-gal) of microglia, and increased expression of senescence associated secretory phenotype (SASP) cytokines (*Il1b*, *Il18*, *Tnf*, *Il6*) in activated hypothalamic microglia. In the liver, increased *p21* and SASP cytokines were detected, although *p16* and β-gal levels remained unchanged. Importantly, miR-146a expression was significantly downregulated in the hypothalamus following HFD exposure in *WT* mice, while miR-146a knockout (*Mir146a-/-*) mice subjected to HFD showed augmented hypothalamic senescence characterized by higher levels of *p16*, *p21*, and β-gal + microglial cells as compared to *WT* mice. The SASP profile remained similar between *Mir146a-/-* HFD and *WT* HFD mice. Among miR-146a target genes, *smad4* was upregulated the hypothalamus of HFD-fed mice, with a more pronounced increase in the hypothalamus of HFD-fed *Mir146a-/-* mice. Further, treatment with Elo upregulated miR-146a expression in both the hypothalamus and the liver, lowered body weight and improved cognitive function, while reducing senescence markers and SASP cytokines in *WT* HFD mice. These effects were absent in *Mir146a-/-* HFD mice when treated with Elo, indicating the dependence of Elo's therapeutic efficacy on miR-146a.

Conclusion Elocalcitol prevents development of senescence in microglia via modulation of miR-146a expression, while miR-146a provides protection against HFD-induced cellular senescence in the hypothalamus most probably via inhibition of TGF/Smad4 pathway. These findings highlight Elo and miR-146a as promising therapeutic candidates for ameliorating obesity-related neuroinflammation and senescence.

Keywords High-fat diet, Hypothalamus, Microglia, Senescence, miR-146a, Elocalcitol

*Correspondence:
Alexander Zharkovsky
aleksander.zarkovski@ut.ee
Full list of author information is available at the end of the article

Background

The global rise in obesity has become a significant public health problem, and is closely associated with an increased risk of metabolic disorders, such as insulin resistance, cardiovascular diseases, chronic inflammation, cancer, and neuropsychiatric disorders [1–5]. In the brain, the hypothalamus is particularly susceptible in regulating glucose and fat metabolism [6, 7], food intake behavior [8], energy homeostasis [9] and aging [10]. Accordingly, numerous studies have demonstrated the development of neuroinflammation in the hypothalamus in obesity. Unlike inflammation in peripheral tissues, which develops over weeks to months upon HFD feeding in rodent models [11–13], markers of hypothalamic inflammation are elevated within 24 h of HFD exposure [14]. Microglia, the resident immune cells in the brain, respond to saturated fatty acids in hypothalamus with morphological changes, such as appearance of a number of prolonged processes and an enlarged cell body [15, 16]. The resulting neuroinflammation in the hypothalamus may be closely linked to metabolic dysfunction and age-related neurodegenerative diseases, underscoring the importance of studies on molecular mechanisms of HFD induced changes in hypothalamus and microglia.

Central to these metabolic disturbances is the consumption of high-fat diets, which not only contribute to excessive weight gain, but also induces cellular senescence - a state of irreversible growth arrest in tissues involved in lipid metabolism [17–20]. Cellular senescence can be triggered by telomere erosion [21], oxidative stress [22], inflammation [23–25], intracellular accumulation of lipids [26], and metabolic dysfunction [27]. Senescent cells display markers, including telomere-associated DNA damage foci [28], increased activity of lysosomal senescence-associated β-galactosidase [29], and increased expression of the cyclin-dependent kinase inhibitor proteins, $p16I^{nk4a}$ [30] and $p21^{Cip1}$ [31]. In addition, senescent cells secrete several inflammatory cytokines, chemokines, and matrix proteases leading to the senescence associated secretory phenotype, SASP [32, 33]. The pro-inflammatory components of SASP contribute to chronic, systemic, low-grade inflammation, called "inflammaging," which is one of the main risk factors for the development age related diseases [34–36]. It has also been reported that obesity leads to the accumulation of senescent cells in the brain [20, 37, 38].

MicroRNAs are small, non-coding RNAs that downregulate gene expression by binding to the 3′ untranslated region of their target mRNAs, leading to mRNA degradation and translation inhibition and thereby influence various cellular processes [39]. Among others, miR-146a-5p (miR-146a later in this article) is known to suppress inflammatory responses via the suppression of multiple direct targets from the NF-κB pathway in innate and adaptive immune cells, keratinocytes and lung epithelial cells [40–45]. miR-146a also inhibits cell proliferation [46], and regulates senescence and apoptosis in pre-adipocytes [47], as well as targets *Smad4* mRNA, a mediator of TGF-β pathway controlling cellular senescence [48]. In the brain, miR-146a is particularly enriched in microglia cells [49, 50], where it regulates several microglial functions, including inflammatory responses and polarization transitions [51–53]. A previous study has demonstrated that miR-146a overexpression can reduce M1 microglial activation induced by metabolic stress by downregulating NF-κB pathway [54]. However, the role of miR-146a in metabolic stress induced microglial senescence remains unexplored.

It has been previously shown that the anti-inflammatory properties of vitamin D analogs [55, 56] and their ability to modulate miRNA profiles contribute to their therapeutic effects [57–59]. To explore therapeutic strategies to counteract HFD-induced changes in the brain, elocalcitol (Elo), also known as BXL-628, a non-hypercalcemic, fluorinated vitamin D analog was used in this study. Elo is known for its ability to inhibit cell growth and proliferation, while it induces apoptosis [60–62]. Previous research has demonstrated its anti-inflammatory effects, notably inhibition of inflammatory responses in human T cells [63], and reduced infiltration of immune cells and inflammation in non-obese diabetic mice [64]. Given its broad regulatory effects, one can suggest that Elo could also modulate inflammatory pathways in tissues affected by HFD.

In the present study, we aimed to investigate using a murine model of HFD-induced obesity the following: (a) the occurrence of cellular senescence in the hypothalamus and liver tissues, (b) the modulatory role of miR-146a in the progression of senescence, and (c) the protective effects of vitamin D and Elo in preventing cellular senescence associated with obesity. Overall, we aimed to contribute to the understanding of obesity-related metabolic disorders and provide insights into potential therapeutic avenues for obesity-related senescence.

Materials and methods

Animals

The first cohort of six-week-old male C57BL/6J mice was obtained from Envigo RMS B.V. (Horst, Netherlands) and was used to study the effects of a high-fat diet. A second cohort, consisting of C57BL/6J wild-type (*WT*) and *Mir146a-/-* mice (both originally purchased from Jackson Laboratory (Bar Harbor, US)), were housed and bred in the laboratory animal facility at the Institute of Biomedicine and Translational Medicine, University of Tartu.

This cohort was used to study the effects of miR-146a deficiency and Elo intervention. The C57BL/6J *WT* and *Mir146a-/-* cohorts were crossbred during maintenance, and to generate *Mir146a-/-* and corresponding *WT* mice *Mir146a+/-* heterozygous mice were crossed. The resulting offspring were genotyped using the following primer sequences: miR-146a forward primer −5' ACCAGC AGTCCTCTTGATGC 3'; miR-146a reverse primer −3' GACGAGCTGCTTCAAGTTCC 5'. Only male littermates from the same generation were used in the experiments. All experiments were conducted in accordance with the Principles of Laboratory Animal Care (Directive 2010/63/EU). The mice were group-housed under a 12-hour light/dark cycle, with food and water provided ad libitum. The experimental protocol was approved by the Animal Experimentation Committee at the Estonian Ministry of Agriculture (No. 177, 2020 and 1.2–17/166, 2023).

Experimental plan

Two sets of mouse experiments were performed: (1) the effects of a HFD on cellular senescence was studied, and (2) the impact of miR-146a deficiency and Elo treatment was investigated. In the first set of experiments, six-week-old C57BL/6J male *WT* mice were divided into two dietary groups: (1) Low-fat diet (LFD) group ($n=19$) received a diet with fat constituting 10% of total energy (3.61 kcal/g), and (2) High-fat diet (HFD) group ($n=19$) received a diet with fat constituting 45% of total energy (4.65 kcal/g). The main source of fat in both diets was lard (ssniff Spezialdiäten GmbH). The mice were fed these diets for 16 weeks and at the age of 24 weeks, after completing behavioral experiments, the animals were euthanized for further analysis. In the second set of experiments, male *WT* ($n=40$) and *Mir146a-/-* ($n=40$) mice were randomly assigned to one of eight experimental groups ($n=10$ per group) to study the effects of miR-146a deficiency and elocalcitol intervention: (1) *WT* mice on a low-fat diet (*WT* LFD), (2) *WT* mice on a high-fat diet (*WT* HFD), (3) *Mir146a-/-* mice on a low-fat diet (*Mir146a-/-* LFD), (4) *Mir146a-/-* mice on a high-fat diet (*Mir146a-/-* HFD), (5) *WT* mice on a low-fat diet with elocalcitol treatment (*WT* LFD + Elo), (6) *WT* mice on a high-fat diet with elocalcitol treatment (*WT* HFD + Elo), (7) *Mir146a-/-* mice on a low-fat diet with elocalcitol treatment (*Mir146a-/-* LFD + Elo), and (8) *Mir146a-/-* mice on a high-fat diet with elocalcitol treatment (*Mir146a-/-* HFD + Elo). Elocalcitol (30 µg/kg, SML2395, Sigma Aldrich, Germany) was administered intraperitoneally twice a week to the respective groups, while others received vehicle. This experimental regimen lasted for eight weeks. Following the dietary and treatment period, behavioral experiments were conducted, after which the animals were euthanized for tissue collection and further analyses. The sequence of the experimental plan is shown in Supplement Fig. 1. The amount of food consumption per cage was measured in cohort 1, while the amount of food consumption per animal was measured in cohort 2. These results are presented in Supplementary Fig. 2.

Body weight and locomotor activity measurement

Body weight and locomotor activity were monitored throughout the duration of the dietary and pharmacological interventions, starting from week 0 and continuing until week 16 for the first cohort, and until week 8 for the second cohort. Locomotor activity was assessed using the PhenoTyper apparatus (Noldus, Leesburg, VA) equipped with EthoVision XT live video tracking software (Version 8.0, Noldus Information Technologies, Leesburg, VA). Mice were individually placed in the PhenoTyper for 30 min during which the total distance traveled within the entire arena was recorded.

Novel object recognition test (NORT)

NORT was performed as described by [65] in an open chamber measuring 50 cm × 50 cm × 50 cm (L × W × H) made of brown wood. The objects used in the test were opaque glass cups with similar textures and colors but varied in size and shape, and were heavy enough to prevent the mice from moving them. The experiment consisted of three phases: habituation, training, and retention. During the habituation phase, mice were allowed to explore the empty arena for 5 min without any objects present, allowing them to become accustomed to the environment. Twenty-four hours after habituation, in the training phase, two identical objects were placed diagonally in the arena, each positioned 10 cm from a corner, and each mouse was allowed to explore the field for 5 min. The time spent exploring both objects was recorded to establish baseline object interaction. Another 24 h later, during the retention phase, mice were introduced to the arena containing one familiar object and one novel object to assess long-term recognition memory. The preference ratio for each mouse was calculated as the percentage of time spent exploring the new object: Preference ratio = (Tnew ×100)/(Tf + Tnew), where Tf and Tnew are the times spent exploring the familiar object and the novel object, respectively. The time spent exploring each object was scored by an observer "blind" to genotypes and in between trials. All of the objects were cleaned with 5% ethanol solution after each trial. Exploration was defined as sniffing or touching the object with the nose or forepaws.

Flow cytometry

Hypothalamic cells were isolated by homogenizing the tissues through 70 µm cell strainers (BD Bioscience) in ice-cold flow buffer (PBS with 1% fetal calf serum). FcR blocking was achieved using mouse FcR blocking reagent (BD Pharmingen™ Purified Rat Anti-Mouse CD16/CD32, Mouse BD Fc Block™). The cells were then stained with anti-mouse CD11b-PerCP/Cy5.5 (Biolegend, cat no. 101228) and CD45-APC (Biolegend, cat no. 103112), along with corresponding isotype control antibodies (rat IgG2b-PerCP/Cy5.5, #400631, and rat IgG2b-APC, #400611) in flow buffer for 1 h. After fixing with 4% paraformaldehyde (PFA) for 10 min at room temperature (RT), the cells were washed to remove the fixative solution. Finally, the cells were stained with the Cell Event Senescence Green flow cytometry assay kit (Thermofisher Scientific, Waltham MA, USA) to detect SA-β-gal in microglial cells according to manufacturer's instructions. Washed and resuspended cells were acquired using a Fortessa flow cytometer (BD Bioscience), and data analysis was performed using Kaluza v2.1 software (Beckman Coulter).

Total RNA isolation and quantitative reverse-transcription PCR (RT-qPCR)

Total RNAs were extracted from the brain (hippocampus, hypothalamus) and liver tissues by using TRI Reagent® (TR 118) (Molecular Research Center, Inc., Cincinati, OH, USA). To measure mRNA expression, cDNA was synthesized using RevertAid First Strand cDNA Synthesis Kit (Thermo Fisher Scientific) followed by qPCR using 5 × HOT FIREPol® EvaGreen® qPCR Supermix (Solis BioDyne, Tartu, Estonia) on a QuantStudio 12KFlex instrument (Thermo Fisher Scientific) according to the instructions of the respective manufacturers. Primer sequences for target genes were given in the Supplement Table 1. Relative miRNA expression was measured using TaqMan® MicroRNA Assays hsa-miR-146a (Assay ID: 000468, Life technologies) according to the manufacturer's instructions. For cRNA synthesis, TaqMan® MicroRNA reverse transcription kit (4366596, Thermo Scientific) and for qPCR, 5× HOT FIREPol® Probe qPCR Mix Plus (ROX) (Solis BioDyne) were used, respectively. U6 snRNA (Assay ID: 001973, Life Technologies) was used for the normalization of RT-qPCR. To analyze relative mRNA expression, ΔΔCt calculations was used. As housekeeping genes for normalization, Gapdh was used. The data were analyzed in relative to the mean value of one of the samples as a calibrator (control sample), which was normalized to 1 and the rest of the samples were compared against the control sample.

Immunohistochemistry of ionized calcium-binding adaptor molecule 1 (Iba1)

Animals were deeply anesthetized with chloral hydrate (300 mg/kg, i.p.) and transcardially perfused using 0.9% saline and then with 4% paraformaldehyde (PFA) in phosphate buffered saline (PBS, pH = 7.4). The brains were kept in PFA solution for 72 h to reduce unspecific binding to endogenous biotin and 40 µm-thick sections were cut on a Leica VT1000S vibro-microtome (Leica Microsystems Pvt Ltd., Wetzlar, Germany) and stored at − 20 °C in the cryo-protectant (30% ethylene glycol, 30% glycerol in PBS: pH 7.4). Before staining, the sections were washed three times in PBS and treated with 2% H2O2 solution for 20 min followed by incubation in 0.01 M citrate buffer (pH 6.0) at 85 °C for 30 min in water bath and then stood for 30 min at RT. Another wash was done in PBS containing 0.1% Triton X-100. Blocking was done with solution containing 5% goat serum, 0.5% Tween-20, 0.25% Triton X-100 in 100 mM PBS for 1 h. Iba1 primary antibody (1: 700, rabbit anti-Iba1, CAF6806, FUJIFILM Wako Chemicals Europe GmbH, Neuss, Germany) was added in blocking buffer for 72 h. After being washed three times, the sections were incubated with secondary antibody (1:700, affinity purified goat anti-rabbit biotinylated IgG (H + L), Vector Laboratories) in blocking buffer at RT for 1 h. Iba1-positive cells were visualized using peroxidase method (ABC system and diaminobenzidine as chromogen, Vector Laboratories). The sections were dried, cleared with xylol and cover-slipped with mounting medium (Vector Laboratories, Newark, CA, USA). To control unspecific binding, some sections were used as negative controls, where incubation step with the primary antibody was omitted. The morphological characteristics of Iba1 + microglia (cell size and cell body size), were analyzed using image analysis software (ImageJ 1.48v, http://imagej.nih.gov/ij). Briefly, images were converted into binarized 8-bit format and "adjusted threshold" and "analyze particles" functions were used to apply intensity thresholds and size filter. To measure the total cell size, the threshold was maintained at the level that was automatically provided by the ImageJ program, and size filter of 150 pixels was applied. To measure the total cell body size, the threshold was lowered by 40 points and no size filter was applied. The counts of Iba-1 positive cells were obtained from images according to the algorithm described previously [66] using "analyze particles" command in ImageJ software.

Western blot of p16, p21 and beta-galactosidase

Liver tissues were lysed in a TRIS-HCl buffer for protein extraction. The protein concentration was determined using the Bradford reagent kit (Sigma, #B6916). For Western blot analysis, 100 µg of total protein was

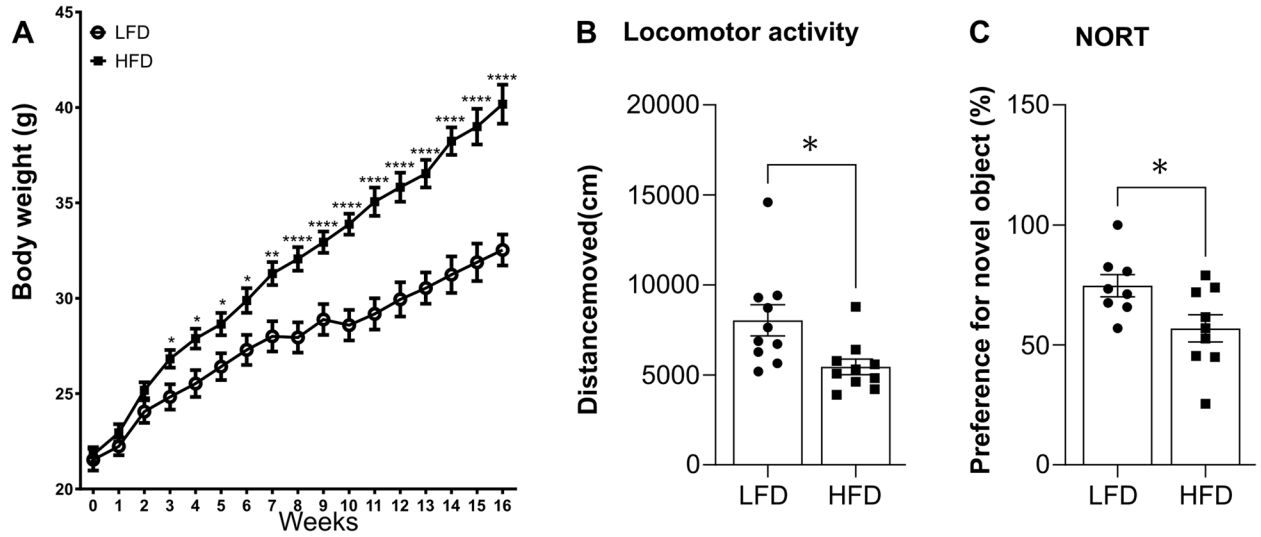

Fig. 1 High-fat diet leads to increased body weight, reduced locomotor activity, and cognitive impairment in mice. The effect of HFD on (**A**) Body weight, (**B**) Locomotor activity, and (**C**) Preference for the novel object. Number of animals = 8–10. Two-way ANOVA followed by Tukey's multiple comparisons test (**A**) and Student's t-test (**B**, **C**). Data are represented as mean ± SEM; *$p < 0.05$, ** $p < 0.01$, *** $p < 0.001$, **** $p < 0.0001$

dissolved in 10% sodium dodecyl sulfate-polyacrylamide gels and transferred electrophoretically onto a nitrocellulose membrane (Millipore). The membranes were blocked with Intercept Blocking Buffer (Li-Cor Biosciences) for 60 min at RT. Afterwards, the blots were incubated for 48 h at 4 °C with primary antibodies for P16 (Rb, #PA5-20379, 1:1000; Invitrogen, USA), P21 (Ms, #sc-6246, 1:1000; Santa Cruz Biotechnology, USA) or beta-galactosidase (Rb, #ab203749, 1:1000; Abcam, UK). After three washes with TBST (50 mmol/L Tris, pH 7.6; 0.9% NaCl; and 0.1% Tween-20), the membranes were incubated for 1 h at RT with the secondary antibody (IRdye800, aMs, #C41028-04 or IRdye800, aRb, #C40721-02, 1:10000; Li-Cor Biosciences). Loading control Gapdh was detected by incubating membranes overnight with monoclonal anti-Gapdh antibody (Ms, ab8245, Abcam; 1:10000), followed by incubation with IRDye conjugated secondary antibody (IRdye680LT, aMs, #C60301-03; 1:10000, Li-Cor Biosciences, USA). Following thorough washing with TBST, antibody detection and quantification were conducted using the Odyssey Infrared Imaging System (Li-Cor Bioscience, USA). Densitometric values for the protein were normalized with GAPDH, and the outcomes were presented as a percentage of the HFD vehicle group.

Statistical analysis

GraphPad 9.4.1 (San Diego, CA, United States) was used for statistical analyses and graphical presentations. All data sets were tested for normal distribution using the Shapiro-Wilk test. If the data sets pass the Shapiro-Wilk test then they were processed using student's t-test or two-way ANOVA followed by Tukey multiple comparisons test. If the data did not pass the Shapiro-Wilk test, they were transformed into logarithms (Y = Log(Y)) and processed further using Mann Whitney test or one-way ANOVA followed by Tukey multiple comparisons test. Statistical significance was set at $p < 0.05$. In all figures, data are shown as mean ± standard error of the mean (SEM). The appropriate statistical test for each data set is specified in the figure legends.

Results

Effects of high-fat diet on body weight, locomotor activity and cognition

To explore the effects of a high-fat diet on behavioral parameters, we subjected mice to HFD and LFD diets and subsequently assessed changes in body weight, locomotor activity, and cognitive function. Mice on HFD exhibited a significant increase in body weight compared to those on the LFD, with this increase becoming significant at week 3rd ($p = 0.0494$) and more pronounced by week 8th ($p < 0.0001$), persisting until the end of the 16th week study period ($p < 0.0001$) (Fig. 1A). Additionally, mice in the HFD group showed significantly reduced locomotor activity compared to those in the LFD group ($p = 0.0156$) (Fig. 1B). The novel object recognition test revealed that the HFD group displayed a decrease in the preference ratio for the novel object ($p = 0.0294$), indicating a decline in cognitive performance compared to the

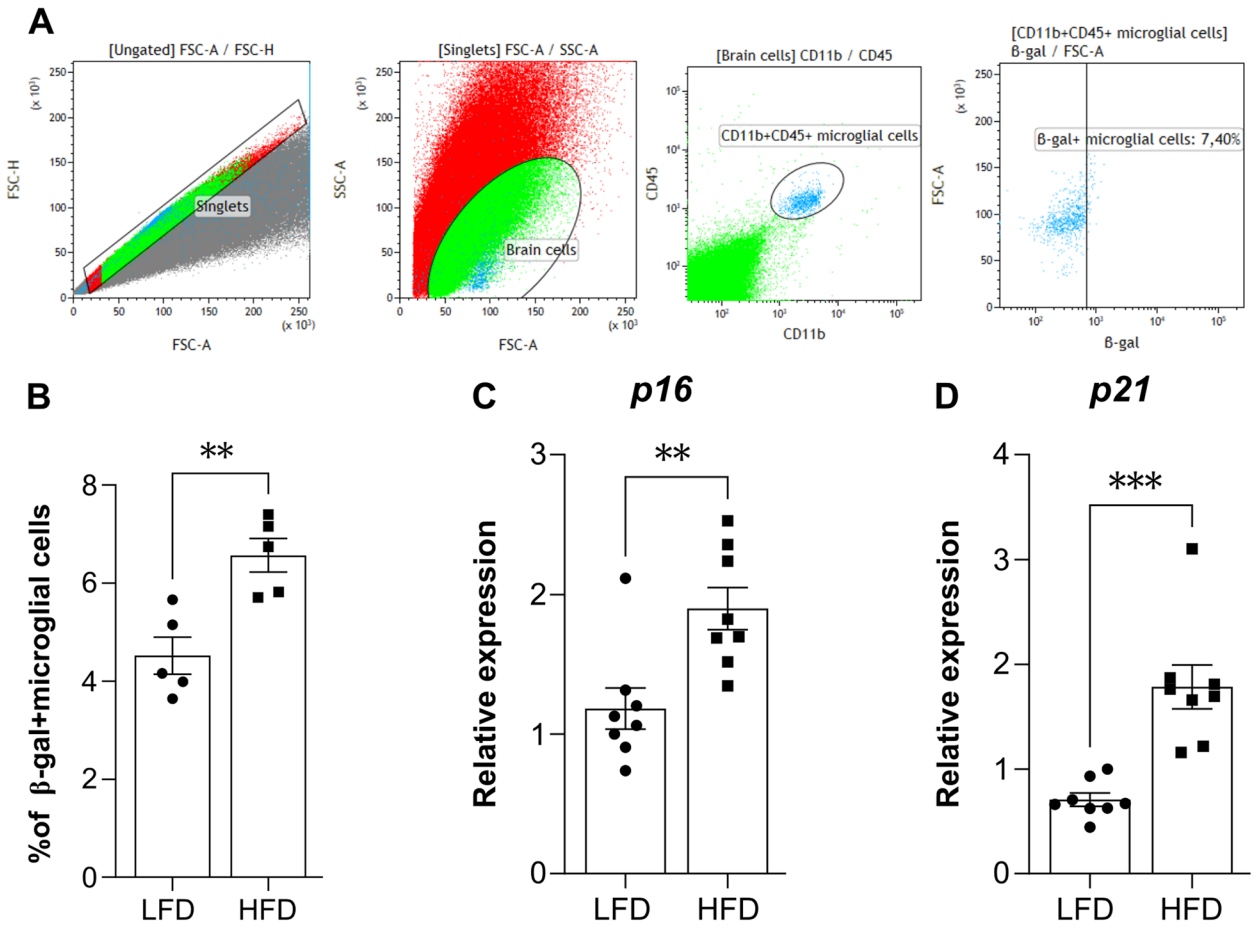

Fig. 2 High-fat diet induces senescence in the hypothalamus. (**A**) Representative dot plots of flow cytometry showing β-gal positive CD45 + CD11b + microglial cells. (**B**) Quantification of β-gal positive CD45 + CD11b + microglial cells in the hypothalamus. (**C**-**D**) RT-qPCR analysis of *p16* and *p21* mRNA expression. Number of animals = 5–8. Student's t-test (**A**, **C**) and Mann Whitney test (**B**). Data are presented as mean ± SEM; ** $p < 0.01$, *** $p < 0.001$

LFD group (Fig. 1C). These results demonstrate that HFD leads to increased body weight, reduced locomotor activity, and impaired cognitive function in mice, underscoring the negative impact of HFD on metabolic and mental health.

High-fat diet leads to increased senescence markers in the hypothalamus of the mouse brain

HFD has been previously shown to induce senescence in the brain [37]. To explore this in our model, we measured senescence-associated β-gal activity specifically in microglial cells using flow cytometry and assessed *p16* and *p21* mRNA expression by RT-qPCR in hypothalamic tissue. To identify β-gal + microglial cells, cells were additionally stained with CD11b and CD45 before staining with β-gal. The gating strategy for the quantification of microglial percentage is shown in Fig. 2A, and a representative of isotypic controls is shown in Supplementary Fig. 3. The hypothalamus showed a significant increase in β-gal positive CD45 + CD11b + microglial cells in the HFD group compared to the LFD group ($p = 0.0040$) (Fig. 2B). Additionally, mRNA expression levels of the senescence markers *p16* and *p21* were significantly elevated in the hypothalamus of HFD-fed mice compared to those on the LFD ($p = 0.0043$, $p = 0.0002$) (Fig. 2C, D). In the hippocampus, no significant changes in *p16*, and *p21* mRNA expression in the HFD group compared to the LFD group was detected (Supplement Fig. 4A and B). These findings indicate that the HFD induced pronounced senescence is restricted to the hypothalamus.

HFD promotes microglial activation and increases SASP cytokines in the hypothalamus

High fat diet is known to induce neuroinflammation and activate microglial cells in the brain [67, 68]. To investigate the effects of HFD on microglial activation and SASP cytokine expression in the hypothalamus, we performed immunostaining, morphological assessment,

and RT-qPCR for mRNA expression of SASP cytokines. First, we measured microglial density and morphology in different hypothalamic regions, including the arcuate nucleus (AN), ventromedial nucleus (VMN), and dorsomedial nucleus (DMN). In both the VMN and DMN, there were no significant differences in microglial density or morphology between the HFD and LFD groups (data not shown). However, in the AN, microglial density was significantly higher in the HFD group compared to the LFD, indicating increased microglial activation in response to HFD ($p=0.0317$) (Fig. 3A, B). Furthermore, morphological analysis in the AN showed that both microglial cell size and cell body size were significantly larger in the HFD group ($p=0.0114$, $p=0.0151$) (Fig. 3C, D), further supporting the presence of microglial activation. In addition, we found increased expression of SASP cytokines, including *Il1b* ($p=0.0012$), *Il18* ($p=0.0008$), *Tnf* ($p=0.0003$) and *Il6* ($p=0.0051$) in the hypothalamus of HFD-fed mice (Fig. 3E-H), indicating a pronounced inflammatory response. These results demonstrate that HFD induces microglial activation and the expression of SASP cytokines in the hypothalamus, contributing to neuroinflammation and the senescent phenotype.

HFD induces early phase senescence markers and SASP cytokines in the liver

The liver is a key organ in metabolism and is highly susceptible to diet-induced changes [69]. HFD is known to induce non-alcoholic fatty liver disease, which is characterized by fat accumulation, inflammation, fibrosis and senescence [70, 71]. To assess the impact of HFD on liver senescence markers in our model, we measured the mRNA and protein levels of p16 and p21 revealing that p16 levels remained unchanged in HFD group compared to LFD group (Fig. 4A, B). In contrast, p21, a marker associated with the initial stages of cellular senescence, exhibited significant increases in both RT-qPCR ($p=0.0011$) and western blot ($p=0.0032$) (Fig. 4C, D), suggesting a selective activation of p21 under HFD conditions. No significant changes were observed in β-galactosidase activity in western blot analysis (Supplementary Fig. 5A). RT-qPCR for SASP cytokines showed significant increase in *Il18* ($p=0.0022$), *Tnf* ($p=0.0079$), and *Il6* ($p=0.0264$) in the liver of HFD-fed mice (Fig. 4E-G), while *Il1b* levels remained the same (Supplementary Fig. 5B). Collectively, these results indicate that HFD leads to increased inflammation in the liver, which may precede senescence state.

HFD induces decreased miR-146a expression in the hypothalamus but not in the liver

Next, we investigated whether miR-146a, a microRNA with well described function in inflammation [72] and senescence [47], is altered in response to a HFD in mice. Our results revealed a significant decrease in miR-146a expression in the hypothalamus of HFD-fed mice compared to those on a LFD ($p=0.0194$) (Fig. 5A). Conversely, miR-146a expression in the liver showed no significant difference between the HFD and LFD groups ($p=0.4463$) (Fig. 5B). These results suggest that downregulation of miR-146a in response to HFD is specific to hypothalamus.

Impact of high-fat diet on body weight, cognitive function, and senescence markers in miR-146a knockout Mice

Since miR-146a expression was significantly altered in response to HFD, we next aimed to understand the role of miR-146a in HFD conditions by comparing *WT* and miR-146a knockout mice subjected to HFD. We measured body weight, cognitive function, and senescence markers in the hypothalamus. Both *Mir146a-/-* and *WT* mice showed a significant increase in body weight upon HFD treatment ($p=0.0010$, $p<0.0001$) with no significant genotypic differences observed (Fig. 6A). A significant effect of HFD treatment on body weight was found ($F(1, 36)=51.29$, $p<0.0001$). In novel object recognition test, HFD induced a decreased preference for the novel object in both *Mir146a-/-* and *WT* mice ($p=0.0483$, $p=0.0279$), with no genotypic differences (Fig. 6B). A significant effect of HFD treatment on NORT performance was observed ($F(1, 26)=16.61$, $p=0.0004$). Next, we measured senescence markers in the hypothalamus. Both *p16* and *p21* mRNA levels were significantly increased upon HFD treatment in both in *WT* ($p=0.0025$, $p=0.0033$) and *Mir146a-/-* ($p<0.0001$, $p=0.0002$) mice, with more pronounced effect in *Mir146a-/-* HFD mice compared to *WT* HFD mice ($p=0.0031$ and $p=0.0355$, respectively) (Fig. 6C, D). A significant effect of HFD treatment on *p16* mRNA expression ($F(1, 16)=69.75$, $p<0.0001$) and on *p21* mRNA expression ($F(1, 16)=47.95$, $p<0.0001$), with a significant genotype effect for both *p16* ($F(1, 16)=14.44$, $p=0.0016$) and *p21* ($F(1, 16)=11.14$, $p=0.0042$) and significant interaction on *p16* ($F(1, 16)=4.862$, $p=0.0424$) was found. Flow cytometry analysis showed an increase in β-gal positive microglial cells in the hypothalamus of *WT* and *Mir146a-/-* upon HFD ($p=0.0445$, $p=0.0004$), with more increase in *Mir146a-/-* HFD compared to *WT* HFD mice ($p=0.0479$) (Fig. 6E). A significant effect of HFD treatment on β-gal positive microglial cells ($F(3, 14)=14.93$, $p=0.0001$) was found. Finally, we measured SASP cytokines. *Il1b*, *Il18*, and *Il6* mRNA levels were significantly increased in the HFD groups compared to the LFD groups in *WT* ($p=0.0016$, $p=0.0064$, $p=0.0244$) and *Mir146a-/-* ($p=0.0171$, $p=0.0027$, $p=0.0159$), with no genotypic differences (Fig. 6F-H). A significant effect of HFD treatment on *Il1b* ($F(3, 15)=11.36$, $p=0.0004$), *Il18*

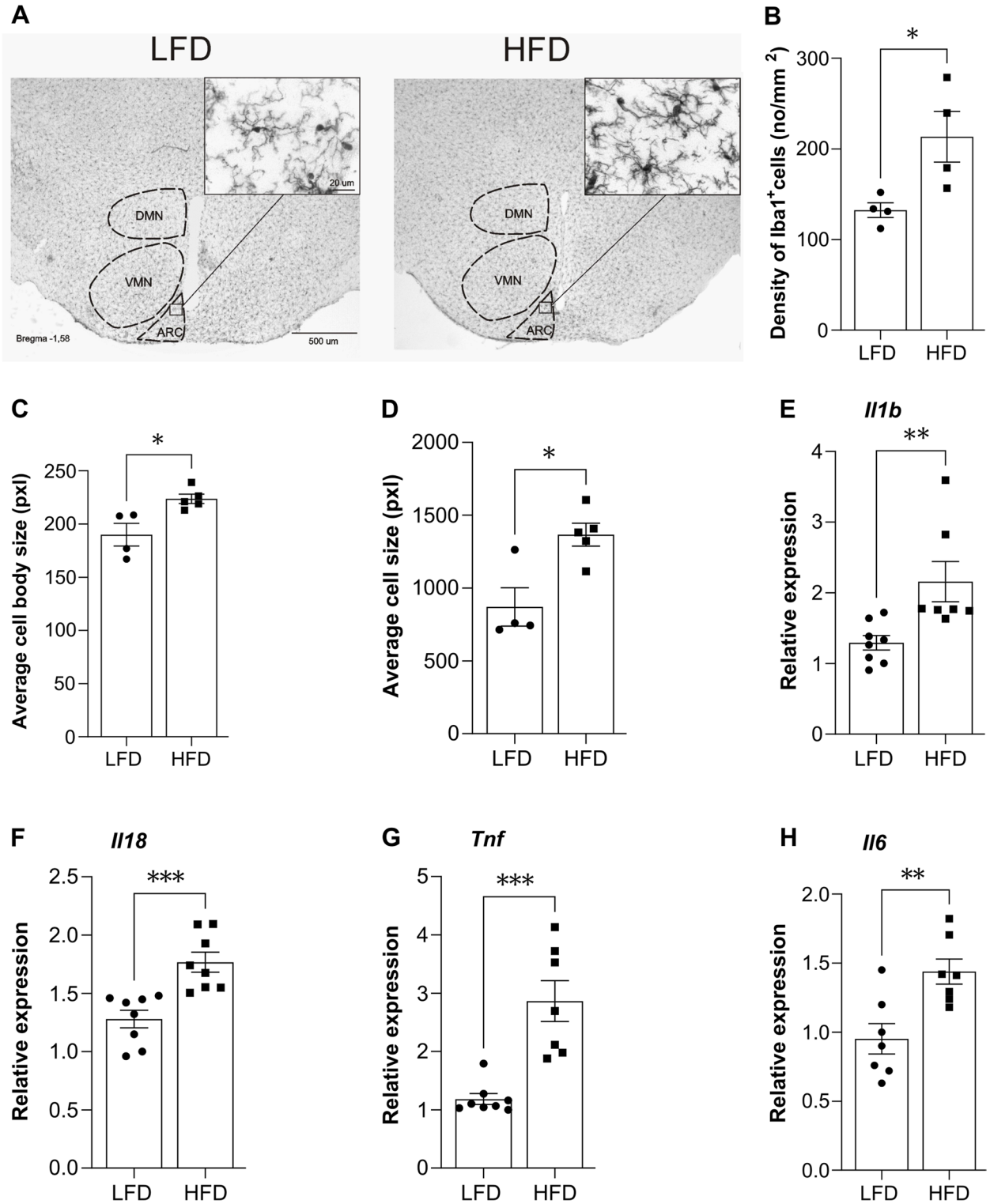

Fig. 3 Microglial activation and elevated SASP cytokines in the hypothalamus induced by HFD. (**A**) Representative immunohistochemistry microphotographs of the hypothalamic Iba1 + cells. (**B**) Density of microglial cells. (**C**) Average cell size of microglial cells. (**D**) Average cell body size of Iba1 + cells in the hypothalamus. (**E**) Relative mRNA expression of *Il1b* (**F**) *Il18* (**G**) *Tnf* and (**H**) *Il6* was analyzed by RT-qPCR with primers for indicated genes. Number of animals = 4–8. Student's t-test (**B**, **C**, **F**, **H**) and Mann Whitney test (**D**, **E**, **G**). Data represented as mean ± SEM; * $p < 0.05$, ** $p < 0.01$, *** $p < 0.001$

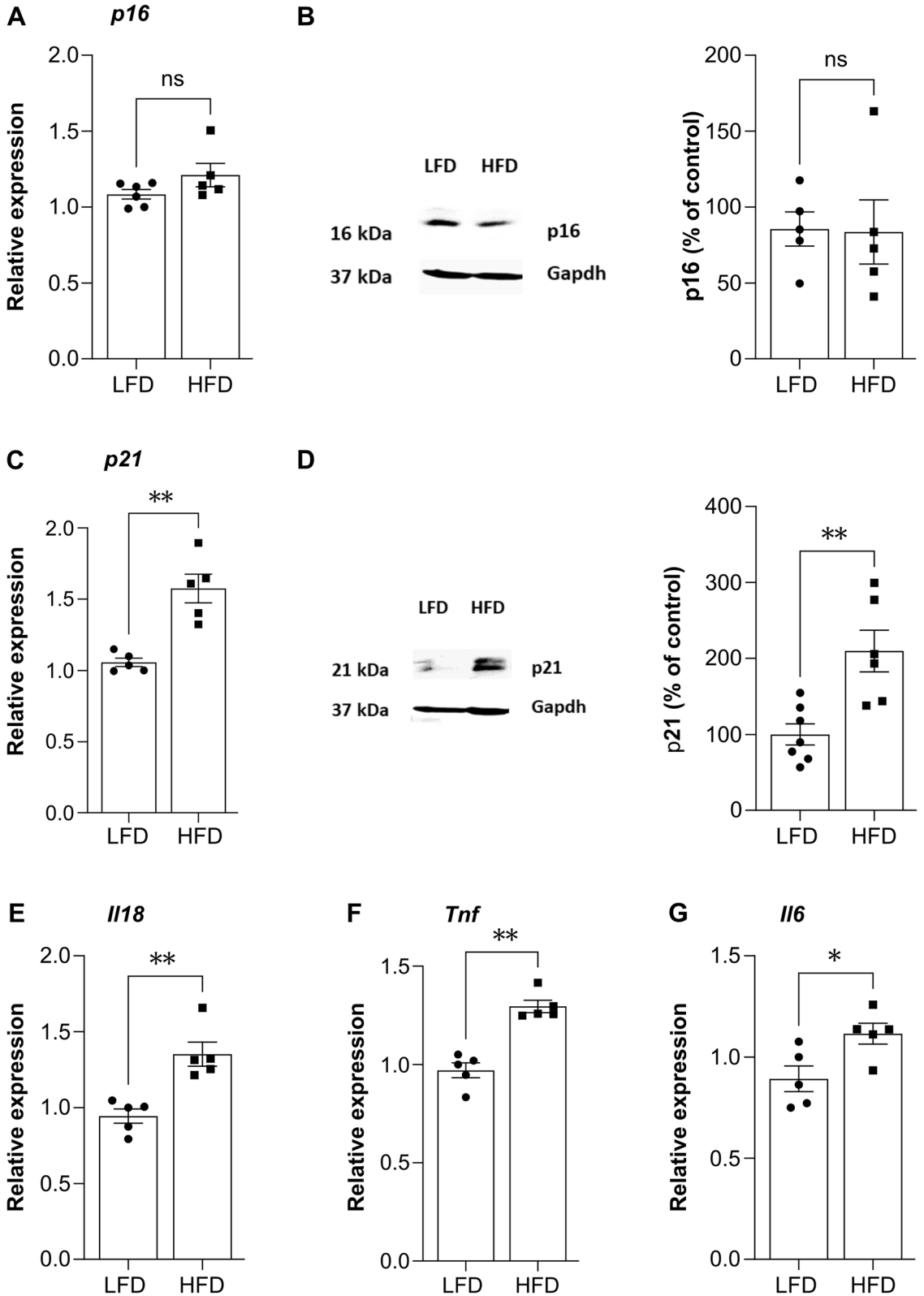

Fig. 4 High-fat diet induces senescence-associated changes and SASP cytokines in the liver. (**A**-**B**) Relative mRNA expression and protein levels of p16, (**C**-**D**) Relative mRNA expression and protein levels of p21 and (**E**-**G**) Relative mRNA expression of *Il18*, *Tnf*, *Il6* cytokines, analyzed by RT-qPCR. Number of animals = 5. Student's t-test (**A**-**E**, **G**) and Mann Whitney test (**F**). Data represented as mean ± SEM; * $p < 0.05$, ** $p < 0.01$, *** $p < 0.001$

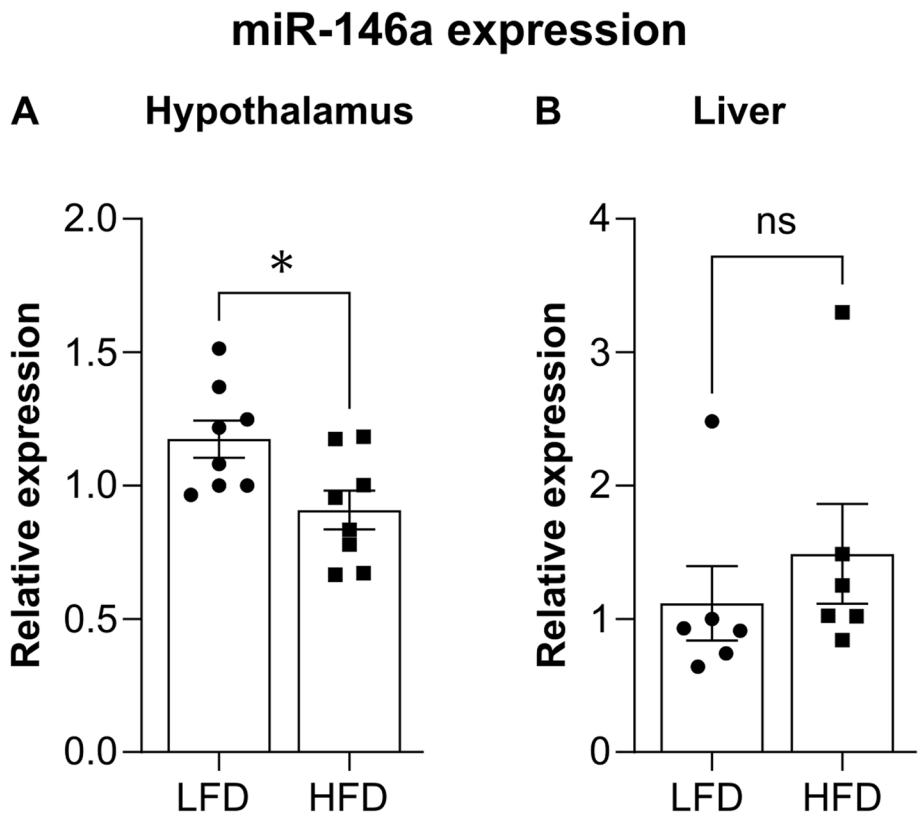

Fig. 5 HFD leads to decreased miR-146a expression in the hypothalamus. (**A**) Relative expression of miR-146a in the hypothalamus and (**B**) liver of LFD and HFD treated groups. Number of animals = 6–8. Data was analyzed using student's t-test and represented as mean ± SEM; *$p < 0.05$

(F (1, 15) = 34.77, $p < 0.0001$), and *Il6* (F (1, 15) = 22.69, $p = 0.0003$) mRNA expression was found. There was no change in *Tnf* expression upon HFD treatment, and no significant genotypic differences were observed (Supplementary Fig. 6). In summary, while both *Mir146a-/-* and *WT* mice displayed similar increase in body weight and cognitive decline under HFD, the absence of miR-146a led to a more pronounced elevation in senescence markers in the hypothalamus, suggesting that miR-146a modulates the extent of senescence induced by HFD.

HFD-induced senescence markers and SASP cytokines in the liver of *WT* and *Mir146a-/-* mice

To further explore the impact of miR-146a deficiency on senescence in liver under HFD conditions, we measured the mRNA expression of senescence markers and SASP cytokines in the liver of both *Mir146a-/-* and *WT* mice. *p16* mRNA expression did not show a significant change between HFD-fed and LFD-fed groups in either *WT* or *Mir146a-/-* mice (Fig. 7A). However, *p21* mRNA levels were significantly elevated in the HFD group compared to the LFD group in *WT* ($p = 0.0089$) and *Mir146a-/-* mice ($p = 0.0108$), with no significant difference between *WT* and *Mir146a-/-* HFD mice (Fig. 7B). A significant effect of HFD treatment on *p21* mRNA expression was observed (F (3, 16) = 9.896, $p = 0.0006$).

Among SASP cytokines, *Il18*, *Tnf*, and *Il6* were significantly upregulated in response to HFD in *WT* ($p = 0.0299$, $p = 0.0392$, $p = 0.0204$) and *Mir146a-/-* mice ($p = 0.0057$, $p = 0.0127$, $p = 0.0690$) with no genotypic

(See figure on next page.)

Fig. 6 Effects of HFD on body weight, cognition and senescence markers in miR-146a knockout mice. (**A**) Body weight changes and (**B**) Preference ratio for the novel object on the novel object recognition test of *WT* and *Mir146a-/-* mice on HFD and LFD. (**C**, **D**) RT-qPCR analysis of *p16* and *p21* mRNA expression levels in the hypothalamus. (**E**) Flow cytometry analysis of β-galactosidase positive microglial cells in the hypothalamus. (**F**-**H**) RT-qPCR analysis of SASP cytokines in *WT* and *Mir146a-/-* mice on HFD and LFD. Number of animals = 4–10. Data panels (**A**-**D**, **G**, **H**) were processed using two-way ANOVA followed by Tukey's multiple comparisons test and (**E**, **F**) were transformed into logarithms (Y = log(Y) and analyzed using one-way ANOVA with Tukey's multiple comparisons test, data in panels. Data are represented as mean ± SEM; * $p < 0.05$, ** $p < 0.01$, *** $p < 0.001$

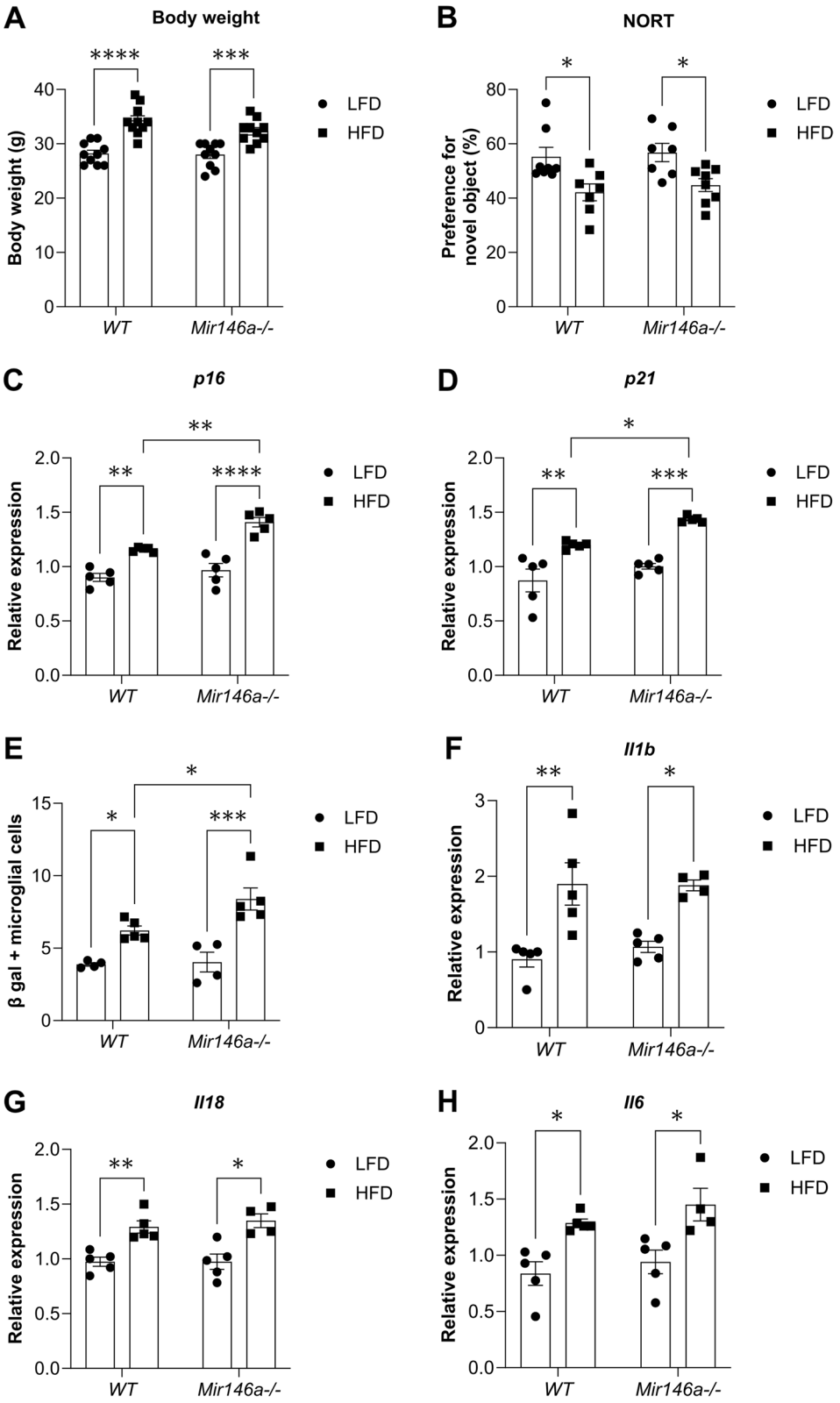

Fig. 6 (See legend on previous page.)

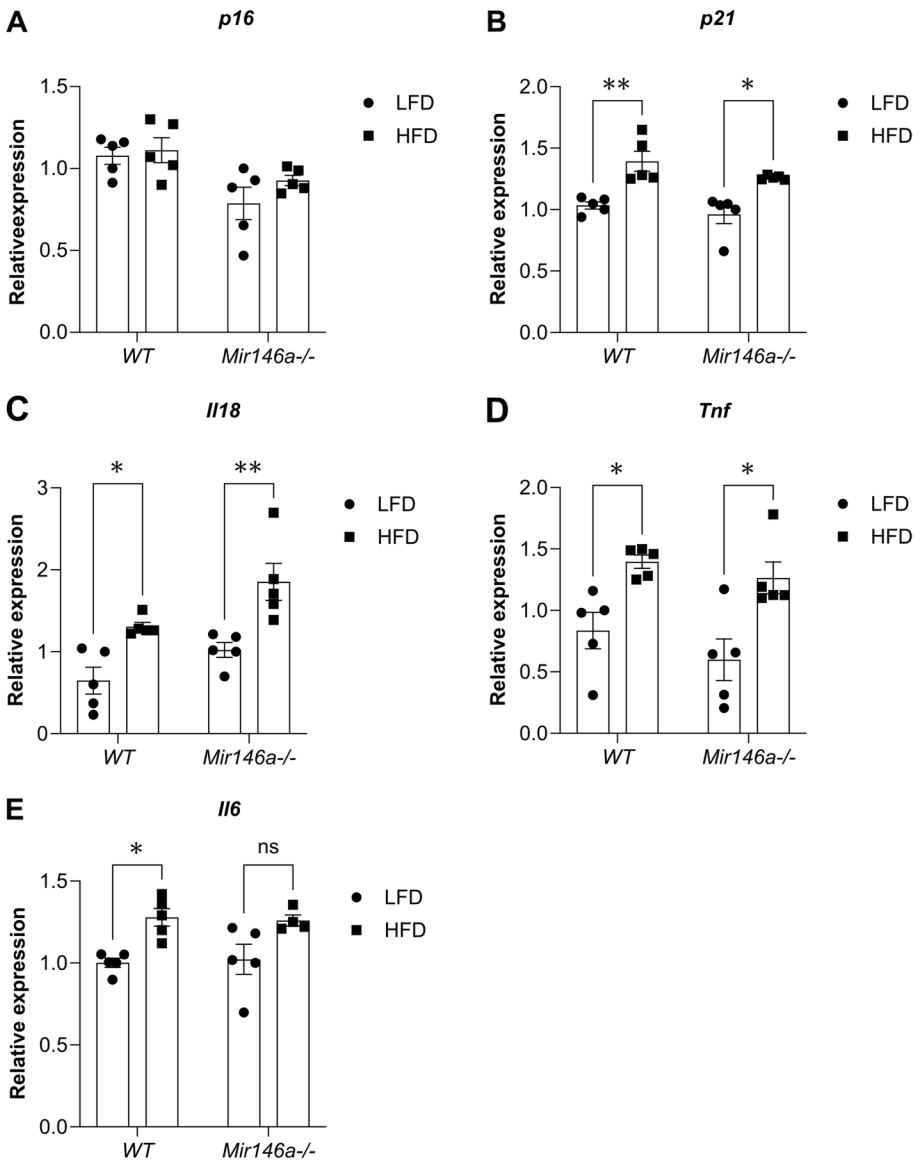

Fig. 7 HFD induces senescence markers and SASP cytokines in the liver of *WT* and *Mir146a-/-* mice. qPCR analysis of (**A**) *p16* mRNA expression, (**B**) *p21* mRNA expression and (**C**-**E**) RT-qPCR analysis of SASP cytokines: *Il18*, *Tnf*, and *Il6* in the liver of *WT* and *Mir146a-/-* mice on HFD and LFD. Number of animals = 5. Data panels (**A**, **C**, **D**, **E**) were analyzed using two-way ANOVA with Tukey's multiple comparisons test, data in panel (**B**) did not pass normality test and transformed into logarithms (Y = log(Y) and further processed using one-way ANOVA with Tukey's multiple comparisons test. Data are represented as mean ± SEM; * $p < 0.05$, ** $p < 0.01$

differences observed (Fig. 7C-E). A significant effect of HFD treatment was found for *Il18* mRNA expression (F (1, 16) = 24.99, $p = 0.0001$), *Tnf* mRNA expression (F (1, 16) = 21.40, $p = 0.0003$), and *Il6* mRNA expression (F (1, 15) = 18.23, $p = 0.0007$). Significant effect of genotype was found only in *Il18* mRNA expression (F (1, 16) = 9.567, $p = 0.0070$). *Il1b* mRNA expression showed no significant change in response to HFD in either genotype (Supplementary Fig. 7). These results indicate that HFD may induce an early phase of senescence in the liver, characterized by increased p21 expression and upregulation of SASP cytokines (*Il18*, *Tnf*, and *Il6*). However, the absence of miR-146a does not significantly alter this response, suggesting that miR-146a may not play a critical role in HFD-induced hepatic senescence and inflammation.

Elevated *Smad4* expression in the hypothalamus of *Mir146a-/-* mice on HFD

To understand the pathways influenced by miR-146a under HFD conditions, we next investigated the mRNA expression of its known targets involved in the regulation of in inflammation and senescence,

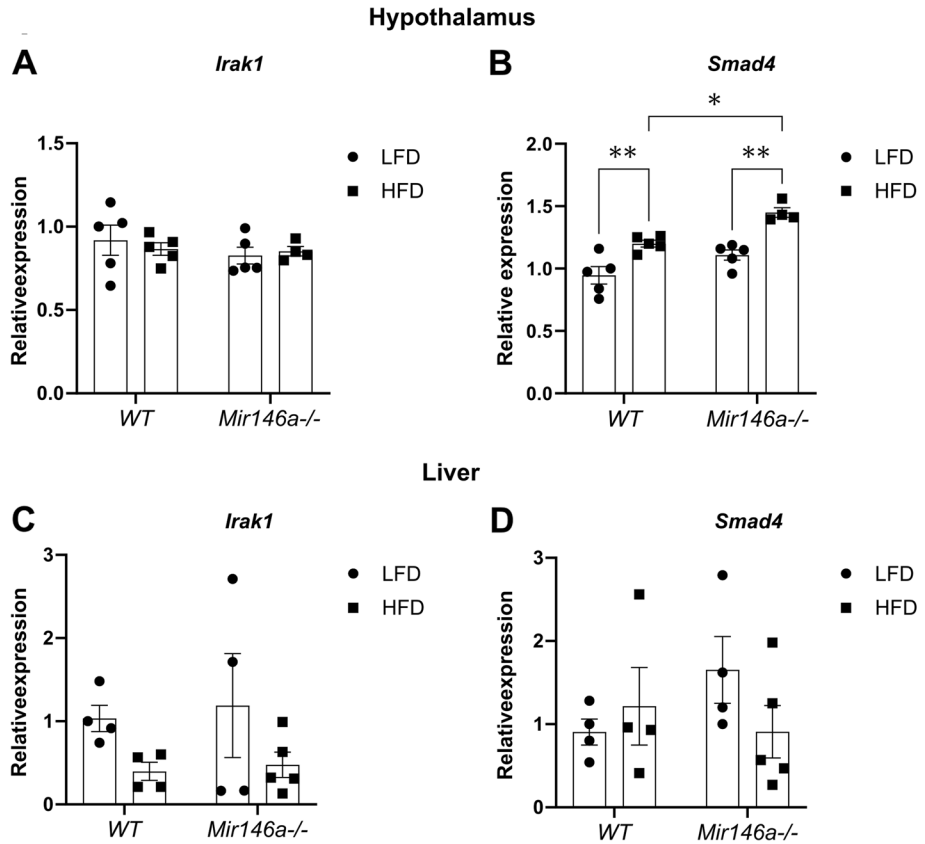

Fig. 8 *Smad4* mRNA expression is increased in the hypothalamus of *Mir146a-/-* mice compared to *WT* mice in HFD conditions. (**A**, **B**) RT-qPCR analysis of *Irak1* and *Smad4* mRNA expression levels in the hypothalamus and (**C**, **D**) liver. Number of animals = 4–6. All data panels were analyzed using two-way ANOVA followed by Tukey's multiple comparisons test. Data are represented as mean ± SEM; * $p < 0.05$, ** $p < 0.01$

such as *Irak1* and *Smad4* [48, 73], in both the hypothalamus and liver. Our analysis revealed that in the hypothalamus, *Irak1* expression showed no significant differences across all groups (Fig. 8A). However, *Smad4* expression was notably elevated in the *WT* HFD group ($p = 0.0074$) compared to the *WT* LFD group and was further increased in the *Mir146a-/-* HFD group compared to the *Mir146a-/-* LFD group ($p = 0.0010$). Additionally, *Smad4* levels were significantly higher in the *Mir146a-/-* HFD group than in the *WT* HFD group ($p = 0.0132$), indicating a more pronounced effect in the absence of miR-146a (Fig. 8B). Significant effect on HFD treatment ($F(1, 15) = 38.57$ $p < 0.0001$) and effects on genotype was found ($F(1, 15) = 18.41$ $p = 0.0006$).

In contrast, no significant changes were observed in the liver for both *Irak1* (Fig. 8C) and *Smad4* (Fig. 8D) across any of the groups, suggesting a tissue-specific regulation by miR-146a, particularly under HFD-induced stress in the brain hypothalamus.

Elocalcitol mitigates HFD-induced behavioral and senescence changes in *WT* mice but not in miR-146a knockout mice

We first investigated the effects of Elo and vitamin D under HFD conditions and observed effects of senescence markers and miR-146a expression. Elo effectively reduced senescence markers *p16* and *p21* in hypothalamus and *p21* in liver (Supplement Fig. 8A–C). While vitamin D under HFD conditions did not show significant effects on these markers. Furthermore, elo significantly upregulated miR-146a in both the hypothalamus and liver, while vitamin D had no significant impact on miR-146a expression under HFD conditions (Supplement Fig. 9A, B). This highlights Elo's ability to mitigate HFD-induced senescence compared to vitamin

D, particularly in regulating miR-146a and senescence-associated pathways.

Next, we assessed whether Elo alone, without HFD, could modulate miR-146a expression. Elo treatment led to a significant increase in miR-146a levels in the hypothalamus (Supplement Fig. 10A) and liver (Supplement Fig. 10B), suggesting that Elo positively modulates miR-146a expression in these key metabolic tissues. To explore the impact of miR-146a modulation on HFD-induced pathologies, we administered Elo to *WT* and *Mir146a-/-* mice on HFD. We then assessed body weight, cognitive function, and senescence markers in the hypothalamus. As shown in Fig. 9A, Elo treatment significantly reduced body weight in the *WT* mice subjected to HFD + Elo compared to *WT* HFD group ($p = 0.0029$). In contrast, the *Mir146a-/-* mice subjected to HFD + Elo did not show a significant reduction in body weight compared to the *Mir146a-/-* HFD group ($p = 0.4032$). Significant effects of Elo treatment (F (3, 36) = 5.695, $p = 0.0027$) was found. Next, assessing the cognitive function using NORT revealed that the *WT* HFD + Elo group exhibited an improved preference for the novel object compared to the *WT* HFD group ($p = 0.0306$). This cognitive benefit was not observed in the *Mir146a-/-* HFD + Elo compared to the *Mir146a-/-* HFD group ($p = 0.7953$) (Fig. 9B). Two-way ANOVA demonstrated significant effects on Elo treatment (F (1, 27) = 7.867, $p = 0.0092$). Next, we assessed the expression of senescence markers in the hypothalamus. *WT* HFD + Elo mice exhibited significantly reduced *p16* mRNA levels compared to *WT* HFD mice ($p = 0.0066$), indicating that Elo attenuates HFD-induced senescence in the hypothalamus. In contrast, *Mir146a-/-* HFD + Elo mice showed no significant changes in *p16* expression compared to *Mir146a-/-* HFD mice ($p = 0.6645$) (Fig. 9C). *p21* mRNA levels also exhibited decreased expression in *WT* HFD + Elo ($p < 0.0001$), but not in *Mir146a-/-* HFD + Elo ($p = 0.9850$) compared to their respective HFD controls (Fig. 9D). One-way ANOVA exhibited significant effects of Elo treatment in both mRNAs *p16* and *p21* (F (3, 16) = 12.65, $p = 0.0002$; F (3, 14) = 25.72, $P < 0.0001$). Flow cytometry revealed that, Elo treatment showed significantly reduced β gal + microglial cells in *WT* HFD + Elo compared to *WT* HFD group ($p = 0.0125$), as expected this change is not observed in *Mir146a-/-* HFD + Elo compared to *Mir146a-/-* HFD group ($p = 0.7652$) (Fig. 9E) and showed significant effect of Elo treatment (F (3, 16) = 13.60, $p = 0.0001$). Analysis of SASP cytokines in the hypothalamus showed a significant decrease in *Il1b* ($p = 0.0057$) (Fig. 9F), *Il18* ($p = 0.0016$) (Fig. 9G) and *Il6* ($p = 0.0390$) (Fig. 9H) in the *WT* HFD + Elo group, not in *Mir146a-/-* HFD + Elo group ($p = 0.6240$, 0.5471, 0.2139) compared to their respective HFD controls. *Il1b*, *Il18* and *Il6* mRNAs were significantly affected by Elo treatment (F (1, 14) = 13.96, $p = 0.0022$; F (3, 15) = 10.11, $p = 0.0007$; F (1, 15) = 12.67, $p = 0.0029$), while *Il6* showed significant effect on genotype (F (1, 15) = 9.121, $p = 0.0086$). Notably, when Elo was administered alone to mice on LFD, there were no significant changes in body weight, cognitive function, senescence markers, or SASP cytokine levels across *WT* and *Mir146a-/-* mice (Data not shown). These findings together suggest that Elo effectively mitigates HFD-induced increases in body weight, cognitive deficits, and senescence markers in *WT* mice. However, these beneficial effects are not observed in *Mir146a-/-* mice, highlighting that miR-146a may have crucial role of in mediating the therapeutic effects of elocalcitol under high-fat diet conditions.

Elocalcitol reduces senescence associated genes and SASP cytokines in the liver in a miR-146a dependent manner

We next also investigated the impact of Elo on liver senescence markers in *WT* and *Mir146a-/-*mice subjected to HFD. First, we assessed the mRNA expression levels of *p16* and *p21*, as well as SASP cytokines, in the liver. We found that *p21* mRNA expression was significantly decreased in the *WT* HFD + Elo group compared to *WT* HFD group ($p = 0.0226$) indicating a potential protective effect of Elo on liver senescence (Fig. 10A). This decrease in *p21* expression was not observed in the *Mir146a-/-* HFD + Elo group ($p = 0.6490$), One-way ANOVA demonstrated significant effect on Elo treatment (F (3, 16) = 4.231, $p = 0.0221$).

Next, we measured the expression of SASP cytokines in the liver. The mRNA levels of *Il18* (F, *Tnf*, and *Il6* were significantly reduced in the *WT* HFD + Elo group

(See figure on next page.)

Fig. 9 Elocalcitol mitigates HFD-induced behavioral and hypothalamic senescence changes in *WT* mice but not in *Mir146a-/-* Mice. (**A**) Body weight changes across four groups: *WT* HFD, *Mir146a-/-* HFD, *WT* HFD + Elo, and *Mir146a-/-* HFD + Elo. (**B**) Preference ratio for the novel object in the novel object recognition test for the same groups. (**C**, **D**) RT-qPCR analysis of *p16* and *p21* mRNA expression levels. (**E**) Flow cytometry analysis of β-galactosidase positive microglial cells in the hypothalamus. (**F**-**H**) RT-qPCR analysis of SASP cytokines in the hypothalamus of *WT* and *Mir146a-/-* mice on HFD and Elo treatment. Number of animals = 4–10. Data panels (**A**, **C**, **D**, **E**, **G**) did not show normal distribution and were transformed into logarithms (Y = log(Y) and analyzed using one-way ANOVA with Tukey's multiple comparisons test and panels (**B**, **F**, **H**) are processed using two-way ANOVA followed by Tukey's multiple comparisons test. Data are represented as mean ± SEM; * $p < 0.05$, ** $p < 0.01$, **** $p < 0.0001$

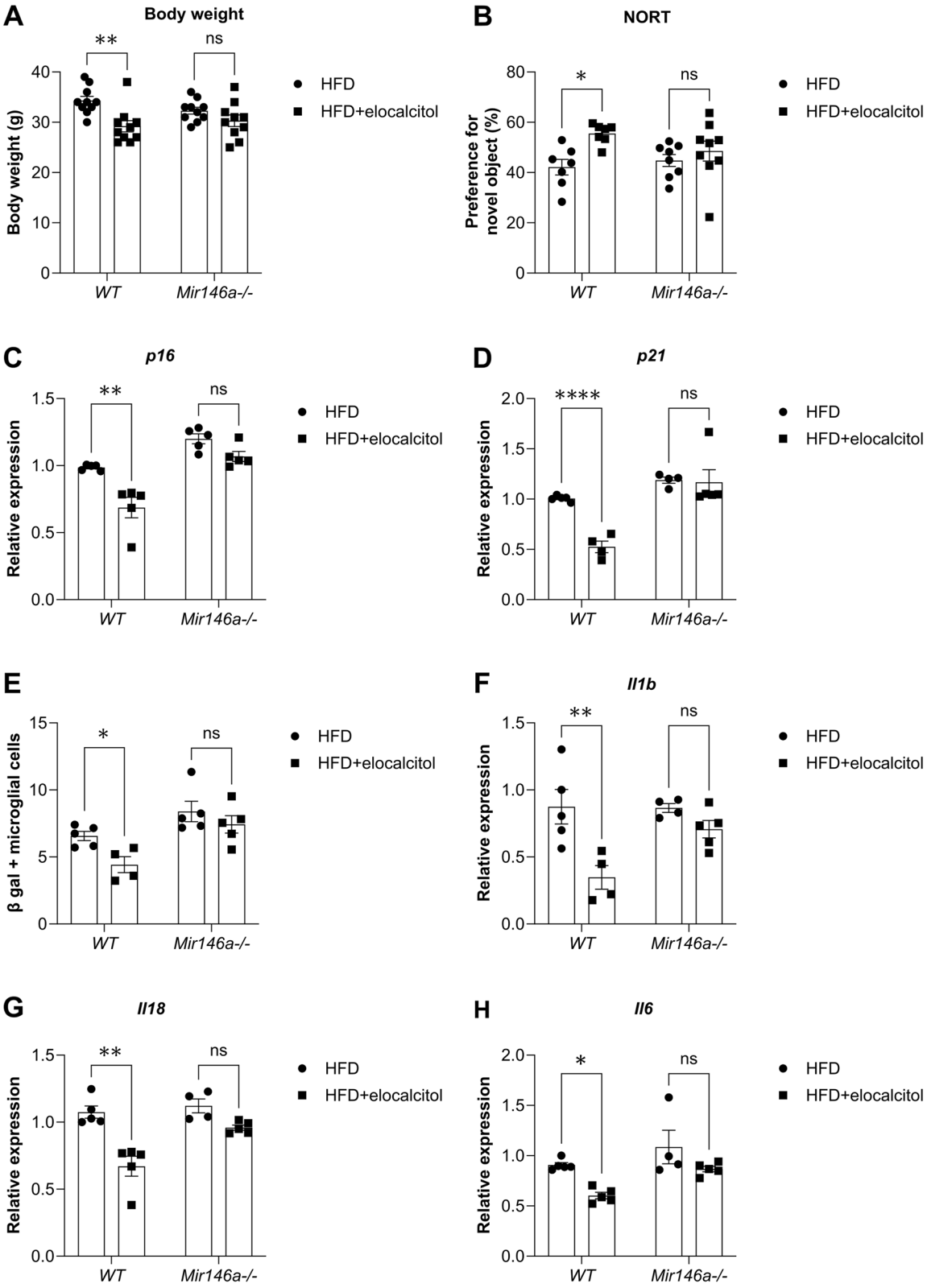

Fig. 9 (See legend on previous page.)

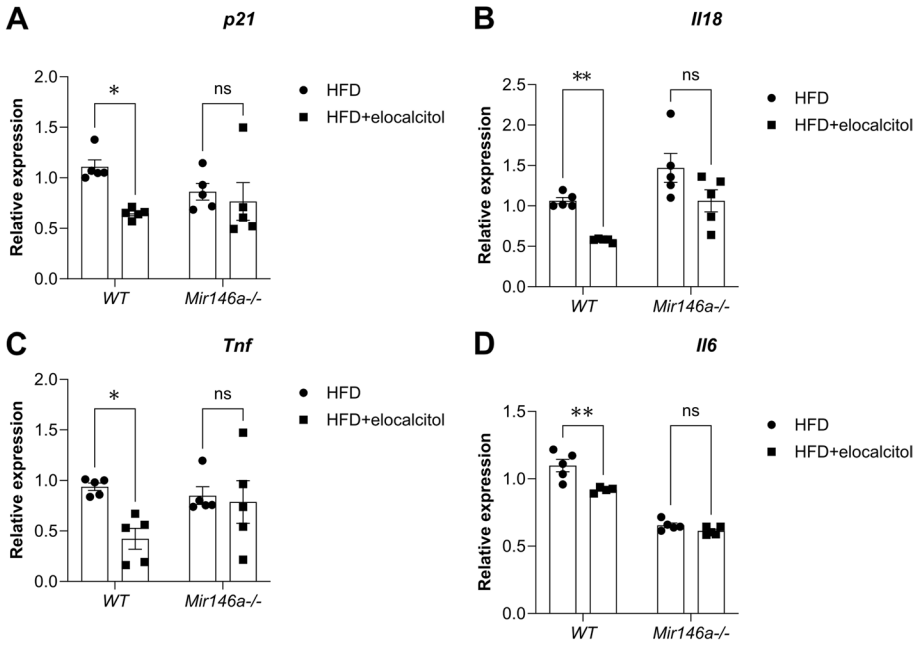

Fig. 10 Elocalcitol reduces HFD-induced senescence and SASP cytokines in liver of *WT* mice but not *Mir146a-/-* mice. (**A**) qPCR analysis of *p21* mRNA expression levels, (**B**) Relative mRNA expression of *Il18*, (**C**) *Tnf*, and (**D**) *Il6* in the liver, analyzed by RT-qPCR with primers for the indicated genes in the liver. Number of animals = 4–5. Data in panels (**A**-**C**) did not show normal distribution and were transformed into logarithms (Y = log(Y) and further processed using one-way ANOVA with Tukey's multiple comparisons test and (**D**) was analyzed using two-way ANOVA followed by Tukey's multiple comparisons test. Data are represented as mean ± SEM; * $p < 0.05$, ** $p < 0.01$

compared to the *WT* HFD group ($p = 0.0013$, $p = 0.0394$, $p = 0.0023$). In contrast, these reductions were not observed in the *Mir146a-/-* HFD + Elo group ($p = 0.0860$, $p = 0.8754$, $p = 0.689$) (Fig. 10B-D). *Il18*, *tnf* and *Il6* mRNA showed significant effects of elocalcitol treatment (F (3, 16) = 17.00, $p < 0.0001$), (F (3, 16) = 3.543, $p = 0.0386$) and (F (1, 15) = 15.99, $p = 0.0012$), while *Il6* mRNA showed significant effect on genotype (F (1, 15) = 183.1, $p < 0.0001$) and interaction (F (1, 15) = 6.247, $p = 0.0245$). Importantly, when Elo was administered alone to mice on an LFD, no significant changes were observed in the expression levels of *p16*, *p21*, or the SASP cytokines across *WT* and *Mir146a-/-* mice (Data not shown). These findings suggest that Elo reduces HFD-induced liver senescence and SASP cytokine expression in a miR-146a-dependent manner.

Discussion

Our study demonstrates that HFD induces pronounced microglial senescence in the hypothalamus, characterized by elevated levels of *p16*, *p21*, and SASP cytokines (*Il1b*, *Il18*, *tnf and Il6*), alongside an increase in β-gal positive microglial cells, indicating an advanced stage of senescence in this brain region. The increased β-gal positive microglial cells in the hypothalamus underscores the advanced nature of senescence in this region, further suggesting that neuroinflammation and cellular aging in the brain are closely linked to dietary-induced metabolic disturbances. The senescent microglial cells likely adopt a senescence-associated secretory phenotype, releasing pro-inflammatory cytokines such as *Il1b*, *Il18*, *Tnf*, and *Il6*. This cytokine production in the hypothalamus suggests that SASP is a central contributor to neuroinflammation under HFD conditions, linking cellular senescence with metabolic stress-induced inflammatory signaling. Notably, there were no significant changes in these markers in the hippocampus, highlighting region-specific responses within the brain. This aligns with existing literature that highlights the sensitivity of hypothalamic neurons and glia to metabolic insults and their pivotal role in the central regulation of energy balance [74, 75]. We also observed increased microglial density upon HFD, which may be a compensatory response to the elevated neuroinflammatory signals associated with senescent cells. Senescent cells release various SASP factors that can attract microglia from other regions, or induce microglial cell proliferation, which might account for the rise in microglial numbers [76, 77]. In line with HFD-induced hypothalamic senescence, cognitive deficits was observed in mice on HFD, as evidenced by decreased preference in the novel object recognition test, a result consistent with previous studies linking

diet-induced obesity to impaired cognitive function [78–80]. These observed cognitive impairments suggest that neuroinflammation and senescence can negatively impact cognitive performance [81].

Our results suggest that HFD may also induced signs of cellular senescence in the liver tissues. This suggestion is supported by the observed elevation of *p21* and SASP cytokines, but in contrast to hypothalamus, the levels of *p16* and β-gal activity remained unchanged. This could indicate that liver senescence is at an initial phase, where cells are beginning to undergo stress-induced premature senescence but have not yet fully transitioned to a senescent state. We speculate that the observed cytokine production in the liver may be driven by stress-induced pathways, such as JNK and STAT3 activation rather than the development of a full SASP response. This distinction suggests that the liver's cytokine response under HFD conditions arises from metabolic stress pathways independent of advanced cellular senescence. The liver's regenerative capacity and different exposure to metabolic factors compared to the brain might also contribute to this delayed or partial senescence response.

The HFD-induced obesity also induced downregulation of miR-146a in hypothalamus but not in liver. Interestingly, although other studies have shown that miR-146a is upregulated in response to obesity and can suppress inflammation in adipose tissue [82], our findings indicate a different pattern of its expression in the brain, specifically the hypothalamus. Another study showed that miR-146a was downregulated in the brain region of the nucleus accumbens under HFD conditions, further suggesting that miR-146a downregulation in response to HFD may be specific to certain brain regions involved in metabolism and reward [83]. The role of miR-146a in the hypothalamic senescence is particularly noteworthy. In the hypothalamus of *Mir146a-/-* HFD mice, we observed an increased expression of senescence markers *p16* and *p21* compared to *WT* HFD mice, indicating that miR-146a may act as a protective factor against HFD-induced cellular senescence specifically in the hypothalamus. This protective effect was not observed in the liver, where the absence of miR-146a did not significantly affect the levels of p21, suggesting that the role of miR-146a in regulating senescence is tissue-specific. The absence of miR-146a removes this regulatory check, consequently, enhanced senescence. Despite the increased senescence markers in *Mir146a-/-* HFD mice, inflammatory cytokine levels (*Il1b*, *Il18*, *Tnf* and *Il6*) were similar between *Mir146a-/-* HFD and *WT* HFD mice. This suggests that while miR-146a plays a significant role in senescence regulation, it does not directly control inflammatory cytokine levels in the same context, pointing to distinct regulatory pathways for senescence and inflammation, and suggesting that miR-146a's influence on senescence may be mediated through mechanisms other than direct cytokine regulation. Our study found no significant differences in body weight gain or cognitive function between *Mir146a-/-* and *WT* mice subjected to HFD treatment. These findings are consistent with previous research indicating that miR-146a deficiency does not affect diet-induced body weight gain [84]. This highlights the tissue-specific roles of miR-146a and suggests that its regulatory effects may differ significantly between central and peripheral tissues.

Our study clearly demonstrated that Elo, a non-hypercalcemic fluorinated analogue of vitamin D, has a protective effect against HFD-induced hypothalamic senescence. Concomitant administration of Elo but not vitamin D prevented impairment of cognition, and reduced the expression of senescence markers and inflammatory cytokines in *WT* mice. By contrast, in animals deficient for miR-146a, Elo failed to prevent body weight gain, cognitive impairments as well as to reduce the expression of senescence markers, this suggests that the protective effects of Elo are mediated, at least in part, through miR-146a pathways. Notably, elo treatment led to upregulation of miR-146a expression in both the hypothalamus and liver, underscoring its role in modulating miRNA expression under metabolic stress conditions. This upregulation of miR-146a could explain the observed reversal of HFD-induced changes in both the hypothalamus and liver, suggesting that Elo may exert its beneficial effects through the restoration of miR-146a levels. Importantly, we are the first to show that Elo can exert reverse cellular senescence, highlighting its potential as a novel therapeutic agent for combating age-related and metabolic disorders. The reduction in senescence markers, such as p16 and p21, and SASP cytokines in both tissues further supports the anti-aging properties of Elo.

To explore which targets of mir-146a might be involved in the regulation of senescence we measured the expression of *Irak1* [72] and *Smad4* [48] in the hypothalamus and liver of *Mir146a-/-* mice and *WT* mice upon HFD treatment. Our data show that *Smad4* mRNA levels were increased in the hypothalamus of HFD mice and even more so in the *Mir146a-/- HFD* group, supporting the hypothesis that miR-146a negatively regulates *Smad4* in the brain. The literature also supports this interaction, showing that miR-146a can target and suppress Smad4, thereby modulating senescence pathways [48]. The heightened levels of *Smad4* in the absence of miR-146a may contribute to the enhanced senescence observed in the hypothalamus of *Mir146a-/-* HFD mice. This aligns with findings that *Smad4* is involved in the regulation of senescence and that its increased expression can lead to the activation of senescence-related pathways.

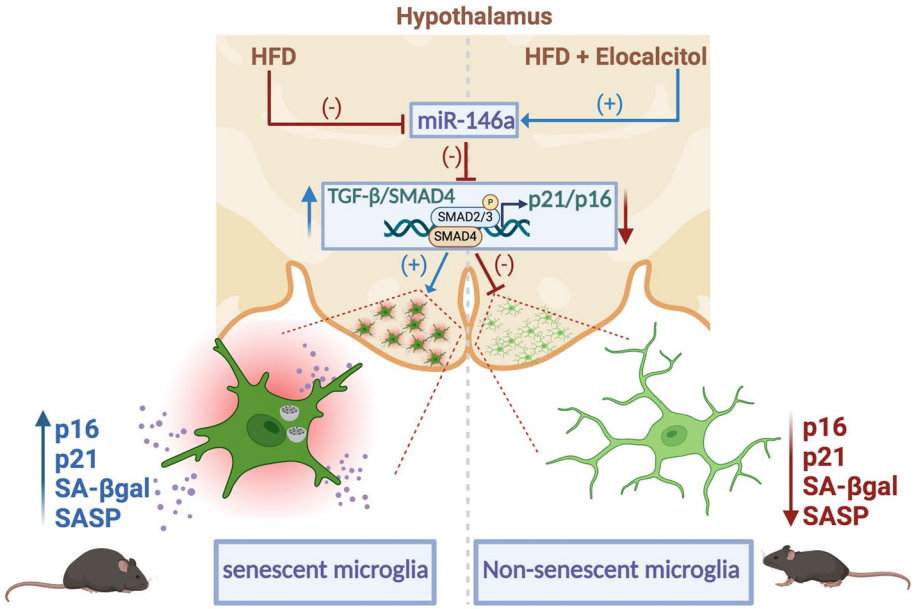

Fig. 11 Role of miR-146a in HFD-induced microglial senescence and the protective effects of elocalcitol. This schematic illustrates the impact of a HFD on miR-146a expression and microglial senescence, as well as the protective effects of elocalcitol treatment. The left side represents the effect of HFD alone, where HFD consumption suppresses miR-146a expression (depicted by the red arrow), which in turn leads to the activation of the TGF-β/SMAD4 pathway. This activation promotes the upregulation of senescence markers (p16, p21), senescence-associated β-galactosidase activity, and the senescence-associated secretory phenotype, contributing to the accumulation of senescent microglia (shown in green with senescence markers and a red halo around them). The right side shows the effects of HFD in combination with elocalcitol treatment. Elocalcitol restores miR-146a expression (depicted by the blue arrow), inhibiting the TGF-β/SMAD4 pathway, and thus reducing the levels of p16 and p21. As a result, SA-βgal activity and SASP are also reduced, which prevents the accumulation of senescent microglia. The microglia are maintained in a non-senescent state (shown with a green outline and no red halo), signifying healthy cellular function. (Created in BioRender. Chithanathan, K. (2024) BioRender.com/w70a352)

However, in the liver, *Smad4* levels did not show significant changes, indicating that miR-146a's regulatory role over *Smad4* is predominantly relevant in the hypothalamus. Interestingly, we found no significant changes in *Irak1* expression in the hypothalamus of either *WT* HFD or *Mir146a-/-* HFD mice, suggesting that while miR-146a might regulate *Irak1* in other tissues, it does not do so in the brain under HFD conditions. Hence, we speculate that downregulating *Smad4*, miR-146a could limit the activation of senescence pathways.

Conclusion

In conclusion, our study shows that HFD-induced hypothalamic senescence is negatively modulated by miR-146a, which appears to play a protective role against senescence by targeting *Smad4* in the hypothalamus. Elocalcitol treatment reverses these effects by restoring miR-146a expression and reducing the activation of senescence markers, as illustrated in Fig. 11. The upregulation of miR-146a by elocalcitol, and its ability to reverse HFD-induced changes in both the liver and hypothalamus, underscores the therapeutic potential of this compound in the context of metabolic and neurodegenerative diseases.

Abbreviations

miRNA	MicroRNA
HFD	High-fat diet
LFD	Low-fat diet
WT	Wild-type
Mir146a-/-	miR-146a knockout
Elocalcitol	Elo
SASP	Senescence-associated secretory phenotype
p16	Cyclin-dependent kinase inhibitor 2 A (CDKN2A)
p21	Cyclin-dependent kinase inhibitor 1 A (CDKN1A)
β-gal	β-galactosidase
Il1β	Interleukin-1 beta
Il6	Interleukin-6
Tnf	Tumor necrosis factor
Il18	Interleukin-18
Smad4	Mothers against decapentaplegic homolog 4
Irak1	Interleukin-1 receptor-associated kinase 1
TGF-β	Transforming growth factor-beta
CNS	Central nervous system
NF-κB	Nuclear factor kappa B
WT LFD	Wild-type mice on a low-fat diet
WT HFD	Wild-type mice on a high-fat diet
Mir146a-/- LFD	miR-146a knockout mice on a low-fat diet
Mir146a-/- HFD	miR-146a knockout mice on a high-fat diet
WT LFD + Elo	Wild-type mice on a low-fat diet with elocalcitol treatment
WT HFD + Elo	Wild-type mice on a high-fat diet with elocalcitol treatment
Mir146a-/- LFD + Elo	miR-146a knockout mice on a low-fat diet with elocalcitol treatment
Mir146a-/- HFD + Elo	miR-146a knockout mice on a high-fat diet with elocalcitol treatment

NORT	Novel object recognition test
Iba1	Ionized calcium-binding adapter molecule 1 (microglial marker)
PFA	Paraformaldehyde
RT	Room temperature
qPCR	Quantitative polymerase chain reaction
SEM	Standard error of the mean

Supplementary Information

The online version contains supplementary material available at https://doi.org/10.1186/s12979-024-00485-6.

Supplementary Material 1.

Authors' contributions

K.C.: Designed and performed qPCR, flow cytometry, western blot, IHC and writing - original draft, Investigation, Formal analysis. M.J.: Established the high-fat diet model, performed behavioral experiments, western blot and IHC. K.D.: Performed RNA isolation and qPCR. A.R.: Performed genotyping. KK: Writing - review & editing. A.R.: Writing - review & editing, Supervision. L.T.: Writing - review & editing, Supervision. A.Z.: Writing – review & editing, Conceptualization, Supervision, Project administration, Funding acquisition.

Funding

AZ is supported by the Estonian Research Council through personal research funding team grant No. PRG878.

Data availability

No datasets were generated or analysed during the current study.

Declarations

Ethics approval and consent to participate

The use of mice was conducted in accordance with the regulations and guidelines approved by the Laboratory Animal Centre at the Institute of Biomedicine and Translational Medicine, University of Tartu, Estonia. All animal procedures were conducted in accordance with the European Communities Directive (2010/63/EU) with permit (No. 177, 2020 and 1.2–17/166, 2023) from the Estonian National Board of Animal Experiments.

Consent for publication

Not applicable.

Competing interests

The authors declare no competing interests.

Author details

[1]Department of Pharmacology, Institute of Biomedicine and Translational Medicine, University of Tartu, Tartu, Estonia. [2]Institute of Science and Technology, University of Tartu, Tartu, Estonia. [3]Department of Biomedicine, Institute of Biomedicine and Translational Medicine, University of Tartu, Tartu, Estonia. [4]Adge Pharmaceuticals Inc, Mountain View, CA, USA. [5]Department of Physiology, Institute of Biomedicine and Translational Medicine, Faculty of Medicine, University of Tartu, Tartu, Estonia.

Received: 2 October 2024 Accepted: 4 November 2024
Published online: 22 November 2024

References

1. Battineni G, Sagaro GG, Chintalapudi N, Amenta F, Tomassoni D, Tayebati SK. Impact of obesity-induced inflammation on cardiovascular diseases (CVD). Int J Mol Sci. 2021;22(9): 4798.
2. Palavra F, Almeida L, Ambrósio AF, Reis F. Obesity and brain inflammation: a focus on multiple sclerosis. Obes Rev. 2016;17(3):211–24.
3. Monteiro R, Azevedo I. Chronic inflammation in obesity and the metabolic syndrome. Mediators Inflamm. 2010;2010:289645.
4. Rohm TV, Meier DT, Olefsky JM, Donath MY. Inflammation in obesity, diabetes, and related disorders. Immunity. 2022;55(1):31–55.
5. Jena PK, Sheng L, Di Lucente J, Jin LW, Maezawa I, Wan YJY. Dysregulated bile acid synthesis and dysbiosis are implicated in Western diet-induced systemic inflammation, microglial activation, and reduced neuroplasticity. FASEB J. 2018;32(5):2866–77.
6. Lee ML, Matsunaga H, Sugiura Y, Hayasaka T, Yamamoto I, Ishimoto T, et al. Prostaglandin in the ventromedial hypothalamus regulates peripheral glucose metabolism. Nat Commun. 2021;12(1):2330.
7. Lam TKT, Pocai A, Gutierrez-Juarez R, Obici S, Bryan J, Aguilar-Bryan L, et al. Hypothalamic sensing of circulating fatty acids is required for glucose homeostasis. Nat Med. 2005;11(3):320–7.
8. Palkovits M. Hypothalamic regulation of food intake. Ideggyogyaszati Szle. 2003;56(9–10):288–302.
9. Williams G, Bing C, Cai XJ, Harrold JA, King PJ, Liu XH. The hypothalamus and the control of energy homeostasis: different circuits, different purposes. Physiol Behav. 2001;74(4–5):683–701.
10. Kim K, Choe HK. Role of hypothalamus in aging and its underlying cellular mechanisms. Mech Ageing Dev. 2019;177:74–9.
11. Kim F, Pham M, Maloney E, Rizzo NO, Morton GJ, Wisse BE, et al. Vascular inflammation, insulin resistance, and reduced nitric oxide production precede the onset of peripheral insulin resistance. Arterioscler Thromb Vasc Biol. 2008;28(11):1982–8.
12. Mori MA, Liu M, Bezy O, Almind K, Shapiro H, Kasif S, et al. A systems biology approach identifies inflammatory abnormalities between mouse strains prior to development of metabolic disease. Diabetes. 2010;59(11):2960–71.
13. Weisberg SP, McCann D, Desai M, Rosenbaum M, Leibel RL, Ferrante AW. Obesity is associated with macrophage accumulation in adipose tissue. J Clin Invest. 2003;112(12):1796–808.
14. Thaler JP, Yi CX, Schur EA, Guyenet SJ, Hwang BH, Dietrich MO, et al. Obesity is associated with hypothalamic injury in rodents and humans. J Clin Invest. 2012;122(1):153–62.
15. Valdearcos M, Robblee MM, Benjamin DI, Nomura DK, Xu AW, Koliwad SK. Microglia dictate the impact of saturated fat consumption on hypothalamic inflammation and neuronal function. Cell Rep. 2014;9(6):2124–38.
16. Baufeld C, Osterloh A, Prokop S, Miller KR, Heppner FL. High-fat diet-induced brain region-specific phenotypic spectrum of CNS resident microglia. Acta Neuropathol (Berl). 2016;132(3):361–75.
17. Sone H, Kagawa Y. Pancreatic beta cell senescence contributes to the pathogenesis of type 2 diabetes in high-fat diet-induced diabetic mice. Diabetologia. 2005;48(1):58–67.
18. Pini M, Czibik G, Sawaki D, Mezdari Z, Braud L, Delmont T, et al. Adipose tissue senescence is mediated by increased ATP content after a short-term high-fat diet exposure. Aging Cell. 2021;20(8):e13421.
19. Li Y, Li X, Xue Q, Wang J, Tan J. High-fat diet and dyslipidemia synergistically contribute to T cell senescence in gut associated lymphoid tissue. Exp Gerontol. 2021;151:111404.
20. Ogrodnik M, Zhu Y, Langhi LGP, Tchkonia T, Krüger P, Fielder E, et al. Obesity-induced cellular senescence drives anxiety and impairs neurogenesis. Cell Metab. 2019;29(5):1061-1077.e8.
21. di d'Adda F, Reaper PM, Clay-Farrace L, Fiegler H, Carr P, Von Zglinicki T, et al. A DNA damage checkpoint response in telomere-initiated senescence. Nature. 2003;426(6963):194–8.
22. Passos JF, Nelson G, Wang C, Richter T, Simillion C, Proctor CJ, et al. Feedback between p21 and reactive oxygen production is necessary for cell senescence. Mol Syst Biol. 2010;6:347.
23. Jurk D, Wilson C, Passos JF, Oakley F, Correia-Melo C, Greaves L, et al. Chronic inflammation induces telomere dysfunction and accelerates ageing in mice. Nat Commun. 2014;2:4172.
24. Li X, Li C, Zhang W, Wang Y, Qian P, Huang H. Inflammation and aging: signaling pathways and intervention therapies. Signal Transduct Target Ther. 2023;8(1):1–29. Available from: https://www.nature.com/articles/s41392-023-01502-8. Cited 2024 Sep 11.
25. Freund A, Orjalo AV, Desprez PY, Campisi J. Inflammatory networks during cellular senescence: causes and consequences. Trends Mol Med. 2010;16(5):238–46. Available from:https://www.ncbi.nlm.nih.gov/pmc/articles/PMC2879478/. Cited 2024 Sep 11.
26. Grepper D, Tabasso C, Aguettaz AKF, Martinotti A, Ebrahimi A, Lagarrigue S, et al. Methodological advancements in organ-specific ectopic lipid

quantitative characterization: effects of high fat diet on muscle and liver intracellular lipids. Mol Metab. 2023;68:101669. Available from: https://www.sciencedirect.com/science/article/pii/S2212877823000030. Cited 2024 Oct 1.
27. Wiley CD, Campisi J. From ancient pathways to aging cells-connecting metabolism and cellular senescence. Cell Metab. 2016;23(6):1013–21.
28. Hewitt G, Jurk D, Marques FDM, Correia-Melo C, Hardy T, Gackowska A, et al. Telomeres are favoured targets of a persistent DNA damage response in ageing and stress-induced senescence. Nat Commun. 2012;3: 708.
29. Dimri GP, Lee X, Basile G, Acosta M, Scott G, Roskelley C, et al. A biomarker that identifies senescent human cells in culture and in aging skin in vivo. Proc Natl Acad Sci U S A. 1995;92(20):9363–7.
30. Serrano M, Lin AW, McCurrach ME, Beach D, Lowe SW. Oncogenic ras provokes premature cell senescence associated with accumulation of p53 and p16INK4a. Cell. 1997;88(5):593–602.
31. Wagner KD, Wagner N. The senescence markers p16INK4A, p14ARF/p19ARF, and p21 in organ development and homeostasis. Cells. 2022;11(12):1966. Available from: https://www.ncbi.nlm.nih.gov/pmc/articles/PMC9221567/. Cited 2024 Sep 11.
32. Coppé JP, Patil CK, Rodier F, Sun Y, Muñoz DP, Goldstein J, et al. Senescence-associated secretory phenotypes reveal cell-nonautonomous functions of oncogenic RAS and the p53 tumor suppressor. PLoS Biol. 2008;6(12):2853–68.
33. Tchkonia T, Zhu Y, van Deursen J, Campisi J, Kirkland JL. Cellular senescence and the senescent secretory phenotype: therapeutic opportunities. J Clin Invest. 2013;123(3):966–72. Available from: https://www.jci.org/articles/view/64098. Cited 2024 Sep 11.
34. Cuollo L, Antonangeli F, Santoni A, Soriani A. The senescence-associated secretory phenotype (SASP) in the challenging future of cancer therapy and age-related diseases. Biology. 2020;9(12): 485.
35. Olivieri F, Prattichizzo F, Grillari J, Balistreri CR. Cellular senescence and inflammaging in age-related diseases. Mediators Inflamm. 2018;2018:9076485.
36. Han X, Lei Q, Xie J, Liu H, Li J, Zhang X, et al. Potential regulators of the senescence-associated secretory phenotype during senescence and aging. J Gerontol Biol Sci Med Sci. 2022;77(11):2207–18.
37. Hou J, Jeon B, Baek J, Yun Y, Kim D, Chang B, et al. High fat diet-induced brain damaging effects through autophagy-mediated senescence, inflammation and apoptosis mitigated by ginsenoside F1-enhanced mixture. J Ginseng Res. 2022;46(1):79–90.
38. Balasubramanian P, Kiss T, Gulej R, Nyul Toth A, Tarantini S, Yabluchanskiy A, et al. Accelerated aging induced by an unhealthy high-fat diet: initial evidence for the role of Nrf2 deficiency and impaired stress resilience in cellular senescence. Nutrients. 2024;16(7): 952.
39. Anglicheau D, Muthukumar T, Suthanthiran M. MicroRNAs: small RNAs with big effects. Transplantation. 2010;90(2):105–12.
40. Taganov KD, Boldin MP, Chang KJ, Baltimore D. NF-kappaB-dependent induction of microRNA miR-146, an inhibitor targeted to signaling proteins of innate immune responses. Proc Natl Acad Sci U S A. 2006;103(33):12481–6.
41. Lu LF, Boldin MP, Chaudhry A, Lin LL, Taganov KD, Hanada T, et al. Function of miR-146a in controlling Treg cell-mediated regulation of Th1 responses. Cell. 2010;142(6):914–29.
42. Boldin MP, Taganov KD, Rao DS, Yang L, Zhao JL, Kalwani M, et al. miR-146a is a significant brake on autoimmunity, myeloproliferation, and cancer in mice. J Exp Med. 2011;208(6):1189–201.
43. Boldin MP, Baltimore D. MicroRNAs, new effectors and regulators of NF-κB. Immunol Rev. 2012;246(1):205–20.
44. Laanesoo A, Urgard E, Periyasamy K, Laan M, Bochkov YA, Aab A, et al. Dual role of the miR-146 family in rhinovirus-induced airway inflammation and allergic asthma exacerbation. Clin Transl Med. 2021;11(6): e427.
45. Hermann H, Runnel T, Aab A, Baurecht H, Rodriguez E, Magilnick N, et al. miR-146b probably assists miRNA-146a in the suppression of keratinocyte proliferation and inflammatory responses in psoriasis. J Invest Dermatol. 2017;137(9):1945–54.
46. Li YL, Wang J, Zhang CY, Shen YQ, Wang HM, Ding L, et al. MiR-146a-5p inhibits cell proliferation and cell cycle progression in NSCLC cell lines by targeting CCND1 and CCND2. Oncotarget. 2016;7(37):59287–98.
47. Nunes ADC, Weigl M, Schneider A, Noureddine S, Yu L, Lahde C, et al. miR-146a-5p modulates cellular senescence and apoptosis in visceral adipose tissue of long-lived Ames dwarf mice and in cultured pre-adipocytes. GeroScience. 2022;44(1):503–18.
48. Min SK, Jung SY, Kang HK, Jo SB, Kim MJ, Min BM. MicroRNA-146a-5p limits elevated TGF-β signal during cell senescence. Mol Ther Nucleic Acids. 2017;7:335–8.
49. Chithanathan K, Somelar K, Jürgenson M, Žarkovskaja T, Periyasamy K, Yan L, et al. Enhanced cognition and neurogenesis in miR-146b deficient mice. Cells. 2022;11(13): 2002.
50. Fregeac J, Moriceau S, Poli A, Nguyen LS, Oury F, Colleaux L. Loss of the neurodevelopmental disease-associated gene miR-146a impairs neural progenitor differentiation and causes learning and memory deficits. Mol Autism. 2020;11(1):1–14.
51. Martin NA, Hyrlov KH, Elkjaer ML, Thygesen EK, Wlodarczyk A, Elbaek KJ, et al. Absence of miRNA-146a differentially alters microglia function and proteome. Front Immunol. 2020;11: 1110.
52. Liu CP, Zhong M, Sun JX, He J, Gao Y, Qin FX. miR–146a reduces depressive behavior by inhibiting microglial activation. Mol Med Rep. 2021;23(6):1–11.
53. Huang Y, Lin X, Lin X. MiR-146a-5p contributes to microglial polarization transitions associated with AGEs. Mol Neurobiol. 2023;60(6):3020–33.
54. Huang Y, Liao Z, Lin X, Wu X, Chen X, Bai X, et al. Overexpression of miR-146a might regulate polarization transitions of BV-2 cells induced by high glucose and glucose fluctuations. Front Endocrinol. 2019;10: 719.
55. Bishop L, Ismailova E, Dimeloe A, Hewison S, White M. Vitamin D and immune regulation: antibacterial, antiviral, anti-inflammatory. JBMR Plus. 2021;5(1):e10405.
56. Chen J, Tang Z, Slominski AT, Li W, Żmijewski MA, Liu Y, et al. Vitamin D and its analogs as anticancer and anti-inflammatory agents. Eur J Med Chem. 2020;207: 112738.
57. Li YC, Chen Y, Liu W, Thadhani R. MicroRNA-mediated mechanism of vitamin D regulation of innate immune response. J Steroid Biochem Mol Biol. 2014;144:81–6 Pt A.
58. Lu'o'ng KVQ, Nguyen LTH. The role of vitamin D in Alzheimer's disease: possible genetic and cell signaling mechanisms. Am J Alzheimers Dis Other Demen. 2013;28(2):126–36.
59. Karkeni E, Bonnet L, Marcotorchino J, Tourniaire F, Astier J, Ye J, et al. Vitamin D limits inflammation-linked microRNA expression in adipocytes in vitro and in vivo: a new mechanism for the regulation of inflammation by vitamin D. Epigenetics. 2018;13(2):156–62.
60. Crescioli C, Ferruzzi P, Caporali A, Scaltriti M, Bettuzzi S, Mancina R, et al. Inhibition of prostate cell growth by BXL-628, a calcitriol analogue selected for a phase II clinical trial in patients with benign prostate hyperplasia. Eur J Endocrinol. 2004;150(4):591–603.
61. Maggi M, Crescioli C, Morelli A, Colli E, Adorini L. Pre-clinical evidence and clinical translation of benign prostatic hyperplasia treatment by the vitamin D receptor agonist BXL-628 (Elocalcitol). J Endocrinol Invest. 2006;29(7):665–74.
62. Marchiani S, Bonaccorsi L, Ferruzzi P, Crescioli C, Muratori M, Adorini L, et al. The vitamin D analogue BXL-628 inhibits growth factor-stimulated proliferation and invasion of DU145 prostate cancer cells. J Cancer Res Clin Oncol. 2006;132(6):408–16.
63. Borgogni E, Sarchielli E, Sottili M, Santarlasci V, Cosmi L, Gelmini S, et al. Elocalcitol inhibits inflammatory responses in human thyroid cells and T cells. Endocrinology. 2008;149(7):3626–34.
64. Penna G, Amuchastegui S, Cossetti C, Aquilano F, Mariani R, Sanvito F, et al. Treatment of experimental autoimmune prostatitis in nonobese diabetic mice by the vitamin D receptor agonist elocalcitol. J Immunol. 2006;177(12):8504–11.
65. Jürgenson M, Aonurm-Helm A, Zharkovsky A. Behavioral profile of mice with impaired cognition in the elevated plus-maze due to a deficiency in neural cell adhesion molecule. Pharmacol Biochem Behav. 2010;96(4):461–8.
66. Jürgenson M, Zharkovskaja T, Noortoots A, Morozova M, Beniashvili A, Zapolski M, et al. Effects of the drug combination memantine and melatonin on impaired memory and brain neuronal deficits in an amyloid-predominant mouse model of Alzheimer's disease. J Pharm Pharmacol. 2019;71(11):1695–705.
67. Ramírez-Carreto RJ, Rodríguez-Cortés YM, Torres-Guerrero H, Chavarría A. Possible implications of obesity-primed microglia that could contribute to stroke-associated damage. Cell Mol Neurobiol. 2023;43(6):2473–90.

68. Spencer SJ, Basri B, Sominsky L, Soch A, Ayala MT, Reineck P, et al. High-fat diet worsens the impact of aging on microglial function and morphology in a region-specific manner. Neurobiol Aging. 2019;74:121–34.
69. Nanizawa E, Otsuka S, Hatayama N, Tamaki Y, Hayashi Y, Ishikawa T, et al. Short-term high-fat and high-carbohydrate diets increase susceptibility to liver injury by inducing hepatic procoagulant and proinflammatory conditions with different balances. Nutrition. 2022;101:111710.
70. Lian CY, Zhai ZZ, Li ZF, Wang L. High fat diet-triggered non-alcoholic fatty liver disease: a review of proposed mechanisms. Chem Biol Interact. 2020;330: 109199.
71. Moustakas II, Katsarou A, Legaki AI, Pyrina I, Ntostoglou K, Papatheodoridi AM, et al. Hepatic senescence accompanies the development of NAFLD in Non-aged mice independently of obesity. Int J Mol Sci. 2021;22(7): 3446.
72. Taganov KD, Boldin MP, Chang KJ, Baltimore D. NF-κB-dependent induction of microRNA miR-146, an inhibitor targeted to signaling proteins of innate immune responses. Proc Natl Acad Sci. 2006;103(33):12481–6.
73. Zhou C, Zhao L, Wang K, Qi Q, Wang M, Yang L, et al. MicroRNA-146a inhibits NF-κB activation and pro-inflammatory cytokine production by regulating IRAK1 expression in THP-1 cells. Exp Ther Med. 2019;18(4):3078–84. Available from: https://www.ncbi.nlm.nih.gov/pmc/articles/PMC6755493/. Cited 2024 Sep 30.
74. Rahman MH, Kim MS, Lee IK, Yu R, Suk K. Interglial crosstalk in obesity-induced hypothalamic inflammation. Front Neurosci. 2018;12: 939.
75. Rodríguez-Rodríguez R, Miralpeix C. Hypothalamic regulation of obesity. Int J Mol Sci. 2021;22(24): 13459.
76. Seguin JA, Brennan J, Mangano E, Hayley S. Proinflammatory cytokines differentially influence adult hippocampal cell proliferation depending upon the route and chronicity of administration. Neuropsychiatr Dis Treat. 2009;5:5–14.
77. Ishijima T, Nakajima K. Inflammatory cytokines TNFα, IL-1β, and IL-6 are induced in endotoxin- stimulated microglia through different signaling cascades. Sci Prog. 2021;104(4): 368504211054985.
78. Zhang Q, Jin K, Chen B, Liu R, Cheng S, Zhang Y, et al. Overnutrition induced cognitive impairment: insulin resistance, gut-brain axis, and neuroinflammation. Front Neurosci. 2022;16: 884579.
79. Dye L, Boyle NB, Champ C, Lawton C. The relationship between obesity and cognitive health and decline. Proc Nutr Soc. 2017;76(4):443–54.
80. Leigh SJ, Morris MJ. Diet, inflammation and the gut microbiome: mechanisms for obesity-associated cognitive impairment. Biochim Biophys Acta Mol Basis Dis. 2020;1866(6):165767.
81. Shafqat A, Khan S, Omer MH, Niaz M, Albalkhi I, AlKattan K, et al. Cellular senescence in brain aging and cognitive decline. Front Aging Neurosci. 2023;15: 1281581.
82. Roos J, Enlund E, Funcke JB, Tews D, Holzmann K, Debatin KM, et al. miR-146a-mediated suppression of the inflammatory response in human adipocytes. Sci Rep. 2016;6(1):1–11.
83. Maldonado-Avilés JG, Guarnieri DJ, Zhu X, DiLeone RJ. Down-regulation of miRNAs in the brain and development of diet-induced obesity. Int J Dev Neurosci. 2018;64:2–7.
84. Javidan A, Jiang W, Okuyama M, Thiagarajan D, Yang L, Moorleghen JJ, et al. miR-146a deficiency accelerates hepatic inflammation without influencing diet-induced obesity in mice. Sci Rep. 2019;9(1):12626.

Publisher's Note